INTERNATIONAL JOURNAL FOR NUMERICAL METHODS IN FLUIDS
Int. J. Numer. Meth. Fluids 2002; **39**:1073–1138 (DOI: 10.1002/fld.346)

Some recent finite volume schemes to compute Euler equations using real gas EOS

T. Gallouët[1,*,†], J.-M. Hérard[1,2] and N. Seguin[1,2]

[1] *Laboratoire d'Analyse Topologie et Probabilités-UMR 6632, Centre de Mathématique et Informatique, Université de Provence, 39 rue Joliot Curie, 13453 Marseille Cedex 13, France*
[2] *Département Mécanique des Fluides et Transferts Thermiques, Électricité de France-Recherche et Développement, 6 quai Watier, 78401 Chatou Cedex, France*

SUMMARY

This paper deals with the resolution by finite volume methods of Euler equations in one space dimension, with real gas state laws (namely, perfect gas EOS, Tammann EOS and Van Der Waals EOS). All tests are of unsteady shock tube type, in order to examine a wide class of solutions, involving Sod shock tube, stationary shock wave, simple contact discontinuity, occurrence of vacuum by double rarefaction wave, propagation of a one-rarefaction wave over 'vacuum', ... Most of the methods computed herein are approximate Godunov solvers: VFRoe, VFFC, VFRoe ncv (τ, u, p) and PVRS. The energy relaxation method with VFRoe ncv (τ, u, p) and Rusanov scheme have been investigated too. Qualitative results are presented or commented for all test cases and numerical rates of convergence on some test cases have been measured for first- and second-order (Runge–Kutta 2 with MUSCL reconstruction) approximations. Note that rates are measured on solutions involving discontinuities, in order to estimate the loss of accuracy due to these discontinuities. Copyright © 2002 John Wiley & Sons, Ltd.

KEY WORDS: finite volume schemes; Euler equations; real gas

1. INTRODUCTION

We discuss in this paper the suitability of some finite volume schemes to compute Euler equations when dealing with real gas state laws, restricting to the one-dimensional framework. Some measured rates of convergence will be presented when focusing on some Riemann problem test cases. This work is based on Reference [1].

Almost all schemes investigated here are approximate Riemann solvers (more exactly approximate Godunov solvers). One may note that comparison with some well-known schemes like Godunov scheme or Roe scheme are not provided in this paper; however, one may refer to References [2–6] for that purpose. Approximate Riemann solvers presented herein may be

*Correspondence to: T. Gallouët, Centre de Mathématique et Informatique, Université de Provence, 39 rue Joliot Curie, 13453 Marseille Cedex 13, France.
†E-mail: gallouet@cmi.univ-mrs.fr

Contract/grant sponsor: Électricité de France (EDF); contract/grant number: C02770/AEE2704

Received December 2000
Revised October 2001

derived using the general formalism of VFRoe ncv scheme. This only requires defining some suitable variable which is not necessarily the conservative variable, but may be defined on the basis of the solution of the Riemann problem for instance. The first one is obviously VFRoe scheme introduced in References [4, 7, 5], where the candidate is the conservative variable. In the second one, which is known as VFFC scheme, and was introduced in References [8–10], the privileged variable is the flux variable. The third one, which was introduced some years ago in Reference [11] and with more details in Reference [12], suggests to consider the ${}^t(\tau, u, p)$ variable in the Euler framework. Extensions of the latter scheme to the frame of shallow water equations, or to some non-conservative hyperbolic systems arising in the 'turbulent' literature are described in References [2, 13, 14]. The fourth one, which applies for the ${}^t(\rho, u, p)$ variable when computing the Euler equations, was introduced by Toro in References [15–17], and is known as PVRS (Primitive Variable Riemann Solver). Note that the latter two rely on (u, p) components, which completely determine the solution of the associated Riemann problem, in the sense that assuming no jump on these in the initial conditions results in 'ghost' 1-wave and 3-wave. Thus the latter two schemes, which are based on the use of u and p variables, are indeed quite different from the other two, since the former requires no knowledge of the one-dimensional Riemann problem solution.

Two slightly different schemes are also used for broader comparison. The first one is the Rusanov scheme [18], which is known to be rather 'diffusive' but anyway enjoys rather pleasant properties, especially when one aims at computing multi-dimensional flows on any kind of unstructured mesh. Recall that for Euler-type systems, this scheme ensures the positivity of mass and species, provided that the 'cell' CFL number is smaller than 1 [19]. Even more, it requires no entropy correction at sonic points in rarefaction waves, when restricting to 'first'-order formulation. The last scheme examined is the energy relaxation method proposed by Coquel and Perthame in Reference [20] (see also References [3, 21] for applications) applied to the frame of VFRoe scheme with ${}^t(\tau, u, p)$ variable. This one again seems appealing both for its simplicity and for its ability to get rid of entropy correction at sonic points in regular fields.

Both 'first-order' schemes and 'second-order' schemes (using RK2 time integration and MUSCL reconstruction with minmod limiter on primitive variables) are examined. This includes three distinct EOS, namely:

- perfect gas EOS,
- Van der Waals EOS,
- Tammann EOS.

Although complex tabulated EOS are not discussed herein, all the above-mentioned schemes enable computation of EOS such as those detailed in References [22] or [23]. Numerous unsteady tests are performed, involving a wide variety of initial conditions, so that the solution may be either a 1-rarefaction wave with a 3-shock wave, a double shock wave or a double rarefaction wave. We give emphasis on symmetric double rarefaction (or shock) waves, since these allow investigation of wall boundary conditions when the standard mirror technique is applied for. The particular experiment of a single isolated contact discontinuity is also described, since the behaviour highly depends on the nature of the state law (see also References [24, 25] on that specific topic). Note also that for almost incompressible fluids, the eigenvalue associated with the LD field is such that the local CFL number varies as $M/(1+M)$, where M stands for the local Mach number, as soon as the overall CFL number is set to 1. As a result, the accuracy of the prediction of the contact discontinuity is rather poor, which is rather annoying since the vapour quality only varies through this field. Eventually, we note that these

test cases include the occurrence of vacuum, and the propagation of a shock wave over a (almost) vacuum of gas. The standard stationary shock is also reported. For completeness, we also refer to Reference [26] where Godunov scheme Reference [27] is used to compute Van Der Waals EOS.

Qualitative behaviour of schemes is discussed, and L^1 error norm is plotted in some cases to provide quantitative comparison. Of course, restricting to smooth solutions, 'first-order' schemes (respectively, 'second-order' schemes) converge at the order 1 (resp. at the order 2), as exposed for instance in References [28, 29]. Solutions investigated here involve some points where the smoothness is only $\mathscr{C}^0$ (at the beginning and at the end of rarefaction waves) and even discontinuities (shocks or contact discontinuities). The quantitative study aims at estimating the rate of convergence in such configurations. Several unsteady solutions are presented:

(i) smooth solutions ($\mathscr{C}^\infty$),
(ii) pure contact discontinuities,
(iii) pure shock waves,
(iv) rarefaction waves connected with constant states (solutions are not $\mathscr{C}^1$),
(v) shock tube test cases which involve several waves.

Both 'first'- and 'second'-order schemes are used on these test cases and associated rates of convergence are measured by refining the mesh (with a constant CFL number).

2. GOVERNING EQUATIONS

2.1. Euler equations under conservative form

Governing Euler equations are written in terms of the mean density ρ, the mean pressure p, the mean velocity u and the total energy E as follows:

$$\frac{\partial W}{\partial t} + \frac{\partial F(W)}{\partial x} = 0 \tag{1}$$

setting

$$W = \begin{pmatrix} \rho \\ \rho u \\ E \end{pmatrix}, \quad F(W) = \begin{pmatrix} \rho u \\ \rho u^2 + p \\ u(E+p) \end{pmatrix} \quad \text{and} \quad E = \rho\left(\frac{1}{2}u^2 + \varepsilon\right)$$

If ε denotes the internal energy, then some law is required to close the whole system

$$p = p(\rho, \varepsilon) \tag{2}$$

such that the Jacobian matrix may be diagonalized in $\mathbb{R}$ for $W \in \Omega$, Ω the set of admissible states, so that $\hat{\gamma}(p,\rho)p > 0$, $\rho > 0$, where

$$\rho c^2(p,\rho) = \hat{\gamma}(p,\rho)p = \left(\frac{\partial \varepsilon}{\partial p_{|\rho}}\right)^{-1}\left(\frac{p}{\rho} - \rho\frac{\partial \varepsilon}{\partial \rho_{|p}}\right)$$

Herein, c stands for the speed of acoustic waves.

The Jacobian matrix $A(W)=\dfrac{\partial F(W)}{\partial W}$ may be written as

$$A(W)=\begin{pmatrix} 0 & 1 & 0 \\ K-u^2 & u(2-k) & k \\ (K-H)u & H-ku^2 & u(1+k) \end{pmatrix}$$

setting

$$H=\frac{E+p}{\rho}$$

$$k=\frac{1}{\rho}\frac{\partial p}{\partial \varepsilon_{|\rho}}$$

$$K=c^2+k(u^2-H)$$

Eigenvalues of the Jacobian matrix $A(W)$ read

$$\lambda_1=u-c, \quad \lambda_2=u, \quad \lambda_3=u+c$$

The associated right eigenvectors are

$$r_1(W)=\begin{pmatrix} 1 \\ u-c \\ H-uc \end{pmatrix}, \quad r_2(W)=\begin{pmatrix} 1 \\ u \\ H-\dfrac{c^2}{k} \end{pmatrix}, \quad r_3(W)=\begin{pmatrix} 1 \\ u+c \\ H+uc \end{pmatrix}$$

Left eigenvectors of $A(W)$ are

$$l_1(W)=\frac{1}{2c^2}\begin{pmatrix} K+uc \\ -ku-c \\ k \end{pmatrix}, \quad l_2(W)=\frac{k}{c^2}\begin{pmatrix} H-u^2 \\ u \\ -1 \end{pmatrix}, \quad l_3(W)=\frac{1}{2c^2}\begin{pmatrix} K-uc \\ -ku+c \\ k \end{pmatrix}$$

Recall that the 1-wave and the 3-wave are genuinely non-linear fields and that the 2-wave is linearly degenerated. In an alternative way, Euler equations may be written in a non-conservative form, when restricting to smooth solutions.

We only provide herein some useful computations of right and left eigenvectors based on non-conservative forms of Euler equations.

2.2. *Non-conservative form wrt* (τ, u, p)

Let us set $\tau=1/\rho$. Thus, Euler equations may be written in terms of (τ, u, p) as

$$\frac{\partial Y_1}{\partial t}+B_1(Y_1)\frac{\partial Y_1}{\partial x}=0$$

with

$$Y_1=\begin{pmatrix}\tau\\ u\\ p\end{pmatrix} \quad \text{and} \quad B_1(Y_1)=\begin{pmatrix}u & -\tau & 0\\ 0 & u & \tau\\ 0 & \hat{\gamma}p & u\end{pmatrix}$$

Obviously, eigenvalues of $B_1(Y_1)$ are still

$$\lambda_1=u-c, \quad \lambda_2=u, \quad \lambda_3=u+c$$

Right eigenvectors of matrix $B_1(Y_1)$ are

$$r_1(Y_1)=\begin{pmatrix}\tau\\ c\\ -\hat{\gamma}p\end{pmatrix}, \quad r_2(Y_1)=\begin{pmatrix}1\\ 0\\ 0\end{pmatrix}, \quad r_3(Y_1)=\begin{pmatrix}\tau\\ -c\\ -\hat{\gamma}p\end{pmatrix}$$

Left eigenvectors of $B_1(Y_1)$ are

$$l_1(Y_1)=\frac{1}{2c^2}\begin{pmatrix}0\\ c\\ -\tau\end{pmatrix}, \quad l_2(Y_1)=\frac{1}{c^2}\begin{pmatrix}1\\ 0\\ \tau^2\end{pmatrix}, \quad l_3(Y_1)=\frac{1}{2c^2}\begin{pmatrix}0\\ -c\\ -\tau\end{pmatrix}$$

2.3. Non-conservative form wrt (ρ, u, p)

In a similar way, we may rewrite Euler equations in terms of (ρ, u, p)

$$\frac{\partial Y_2}{\partial t}+B_2(Y_2)\frac{\partial Y_2}{\partial x}=0$$

with

$$Y_2=\begin{pmatrix}\rho\\ u\\ p\end{pmatrix} \quad \text{et} \quad B_2(Y_2)=\begin{pmatrix}u & \rho & 0\\ 0 & u & \frac{1}{\rho}\\ 0 & \hat{\gamma}p & u\end{pmatrix}$$

Right eigenvectors of $B_2(Y_2)$ are now

$$r_1(Y_2)=\begin{pmatrix}1\\ -\dfrac{c}{\rho}\\ c^2\end{pmatrix}, \quad r_2(Y_2)=\begin{pmatrix}1\\ 0\\ 0\end{pmatrix}, \quad r_3(Y_2)=\begin{pmatrix}1\\ \dfrac{c}{\rho}\\ c^2\end{pmatrix}$$

Meanwhile, left eigenvectors of matrix $B_2(Y_2)$ read

$$l_1(Y_2)=\frac{1}{2c^2}\begin{pmatrix}0\\ -\rho c\\ 1\end{pmatrix}, \quad l_2(Y_2)=\begin{pmatrix}1\\ 0\\ -\frac{1}{c^2}\end{pmatrix}, \quad l_3(Y_2)=\frac{1}{2c^2}\begin{pmatrix}0\\ \rho c\\ 1\end{pmatrix}$$

2.4. Non-conservative form wrt $F(W)$

We may rewrite the above-mentioned equations in terms of the variable $Y=F(W)$. We multiply on the left by $A(W)$ system (1):

$$A(W)\frac{\partial W}{\partial t}+A(W)\frac{\partial F(W)}{\partial x}=0$$

Since $A(W)$ is the Jacobian matrix of flux $F(W)$, we get

$$A(W)\frac{\partial W}{\partial t}=\frac{\partial F(W)}{\partial t}$$

Hence,

$$\frac{\partial F(W)}{\partial t}+A(W)\frac{\partial F(W)}{\partial x}=0$$

The associated matrix still is $A(W)$. The eigenstructure is detailed in Section 2.1. We now describe the three equations of state used in our computations.

2.5. Considering various EOS

2.5.1. Perfect gas EOS. The closure law is

$$p=(\gamma-1)\rho\varepsilon$$

with

$$\gamma=1,4$$

2.5.2. Tammann EOS. This law is sometimes used to describe the thermodynamics of the liquid phase (see [15]). It may be simply written as

$$p=(\gamma_c-1)\rho\varepsilon-\gamma_c p_c$$

where

$$\gamma_c=7,15,\quad p_c=3\times 10^8$$

Actually, using some suitable change of variables enables to retrieve Euler equations with perfect gas state law, assuming $\gamma=\gamma_c$. This is an interesting point, since some schemes benefit from nice properties when restricting to perfect gas EOS (see, for instance, VFRoe with non-conservative variable).

2.5.3. Van Der Waals EOS. Van Der Waals EOS is recalled below:

$$\left(p+\frac{a}{\tau^2}\right)(\tau-b)=RT$$

$$\varepsilon-\varepsilon_0=c_vT-\frac{a}{\tau}$$

$$c^2=-2\frac{a}{\tau}+(p\tau^2+a)\left(1+\frac{R}{c_v}\right)\Big/(\tau-b)$$

where

$$b = 0\,001\,692, \quad R = 461,5$$
$$a = 1684,54, \quad c_v = 1401,88$$
$$\varepsilon_0 = 0$$

This identifies with perfect gas EOS while setting $a = b = 0$. This law enables to exhibit some deficiencies of schemes around the contact discontinuity in some cases. We refer to Reference [26] which provides some approximation based on Godunov scheme, when focusing on this particular EOS. Initial conditions in shock-tube experiments are taken in this reference. Comparison with some other test cases can be found in References [11, 12, 19].

3. NUMERICAL SCHEMES

3.1. Framework

3.1.1. Finite volume schemes. We thus focus herein on some finite volume schemes (see for example References [30, 31]). Regular meshes are considered, whose size Δx is such that: $\Delta x = x_{i+1/2} - x_{i-1/2}$, $i \in \mathbb{Z}$. Let us denote as usual Δt the time step, where $\Delta t = t^{n+1} - t^n$, $n \in \mathbb{N}$.

We denote by $W \in \mathbb{R}^n$ the exact solution of the non-degenerate hyperbolic system:

$$\frac{\partial W}{\partial t} + \frac{\partial F(W)}{\partial x} = 0$$
$$W(x,0) = W_0(x)$$

with $F(W)$ in $\mathbb{R}^n$.

Let W_i^n be the approximate value of $\frac{1}{\Delta x}\int_{x_{i-1/2}}^{x_{i+1/2}} W(x,t^n)\,\mathrm{d}x$.

Integrating over $[x_{i-1/2}; x_{i+1/2}] \times [t^n; t^{n+1}]$ provides

$$W_i^{n+1} = W_i^n - \frac{\Delta t}{\Delta x}(\phi_{i+1/2}^n - \phi_{i-1/2}^n)$$

where $\phi_{i+1/2}^n$ is the numerical flux through the interface $\{x_{i+1/2}\} \times [t^n; t^{n+1}]$. The time step should comply with some CFL condition in order to guarantee non-interaction of numerical waves inside one particular cell, or some other stability requirement. We restrict our presentation to the frame of three point schemes. Thus, $\phi_{i+1/2}^n$ only depends on W_i^n and W_{i+1}^n, namely $\phi_{i+1/2}^n = \phi(W_i^n, W_{i+1}^n)$. Whatever the scheme is, the following consistency relation should hold

$$\phi(V,V) = F(V)$$

Hence, we present now approximate numerical fluxes $\phi(W_L, W_R)$ associated with the 1D Riemann problem

$$\begin{aligned} &\frac{\partial W}{\partial t} + \frac{\partial F(W)}{\partial x} = 0 \\ &W(x,0) = \begin{cases} W_L & \text{if } x<0 \\ W_R & \text{if } x>0 \end{cases} \end{aligned} \tag{3}$$

3.1.2. VFRoe schemes. These are approximate Godunov schemes where the approximate value at the interface between two cells is computed as follows. Let us consider some change of variable $Y=Y(W)$ in such a way that $W_{,Y}(Y)$ is inversible. The counterpart of the above system for regular solutions is

$$\frac{\partial Y}{\partial t} + B(Y)\frac{\partial Y}{\partial x} = 0$$

where $B(Y)=(W_{,Y}(Y))^{-1}A(W(Y))\ W_{,Y}(Y)$ ($A(W)$ stands for the Jacobian matrix of flux $F(W)$).

Now, the numerical flux $\phi(W_L, W_R)$ is obtained solving the linearized hyperbolic system

$$\begin{aligned} &\frac{\partial Y}{\partial t} + B(\hat{Y})\frac{\partial Y}{\partial x} = 0 \\ &Y(x,0) = \begin{cases} Y_L = Y(W_L) & \text{if } x<0 \\ Y_R = Y(W_R) & \text{if } x>0 \end{cases} \end{aligned} \tag{4}$$

where $\hat{Y}$ agrees with condition: $\hat{Y}(Y_L, Y_L)=Y_L$.

Once the exact solution $Y^*(x/t; Y_L, Y_R)$ of this approximate problem is obtained, the numerical flux is

$$\phi(W_L, W_R) = F(W(Y^*(0; Y_L, Y_R)))$$

Notation

In the following we note $\tilde{}$ variables which are computed on the basis of $\overline{Y}$ (obviously, if α is one component of $\overline{Y}$, the relation below holds: $\tilde{\alpha}=\bar{\alpha}$).

Let us set $\widetilde{l_k}$, $\widetilde{\lambda_k}$ and $\widetilde{r_k}$, $k=1,\ldots,n$, left eigenvectors, eigenvalues and right eigenvectors of matrix $B(\overline{Y})$, respectively. If $x/t \neq \lambda_k$, $k=1,\ldots,n$, then the solution $Y^*(x/t; Y_L, Y_R)$ of linear problem is

$$\begin{aligned} Y^*(x/t; Y_L, Y_R) &= Y_L + \sum_{x/t>\widetilde{\lambda_k}} ({}^t\widetilde{l_k}(Y_R - Y_L))\widetilde{r_k} \\ &= Y_R - \sum_{x/t<\widetilde{\lambda_k}} ({}^t\widetilde{l_k}(Y_R - Y_L))\widetilde{r_k} \end{aligned}$$

Let us emphasize that all schemes involved by the VFRoe ncv formalism are approximate Godunov schemes. Note that, contrary to the Godunov scheme, VFRoe ncv schemes cannot

be interpreted as projection methods. Hence, no theoretical result exists to ensure a good behaviour of the algorithm when dealing with simulations including states near vacuum (see Reference [32]).

3.1.3. Entropy correction. When one numerical eigenvalue associated with the 1-wave or the 3-wave vanishes, an entropy correction is needed for the above-mentioned schemes. If a 1-rarefaction wave overlapping the interface is detected, the approximate value at the interface is modified as

$$Y^*(0; Y_L, Y_R) = \frac{Y_L + Y_1}{2}$$

In the first approach [11], we assume that overlapping occurs if

$$\lambda_1(W_L) < 0$$

and if, in addition, $\widetilde{\lambda_1}$ is close to 0.

An alternative way consists in the proposal of Harten and Hyman in Reference [33], thus checking whether

$$\lambda_1(W_L) < 0 < \lambda_1(W_R)$$

This second approach has been applied herein.

3.2. Basic VFRoe scheme

This scheme was first proposed in References [4, 5, 7]. It is based on the following choice $Y(W) = W$ and thus $B(\overline{Y}) = A(\overline{W})$. Recall that $A(W)$ is the Jacobian matrix of $F(W)$ in the linearized Riemann problem.

3.3. VFRoe with non-conservative variable (τ, u, p)

We set now $Y(W) = {}^t(\tau, u, p)$, where $\tau = 1/\rho$. This scheme was introduced in Reference [11] (see also References [2, 12, 14, 19] for various applications).

With the help of left eigenvectors of $B(\overline{Y})$ detailed in Section 2.2, and defining $\tilde{\alpha}_1$ and $\tilde{\alpha}_3$ as

$$\tilde{\alpha}_1 = \frac{1}{2\tilde{c}^2}(\tilde{c}\Delta u - \bar{\tau}\Delta p)$$
$$\tilde{\alpha}_3 = -\frac{1}{2\tilde{c}^2}(\tilde{c}\Delta u + \bar{\tau}\Delta p)$$

where $\Delta(.) = (.)_R - (.)_L$, intermediate states Y_1 and Y_2 read

$$Y_1 = \begin{pmatrix} \tau_L + \tilde{\alpha}_1\bar{\tau} \\ u_L + \tilde{\alpha}_1\tilde{c} \\ p_L - \tilde{\alpha}_1\tilde{\tilde{\gamma}}\bar{p} \end{pmatrix} \quad \text{and} \quad Y_2 = \begin{pmatrix} \tau_R - \tilde{\alpha}_3\bar{\tau} \\ u_R + \tilde{\alpha}_3\tilde{c} \\ p_R + \tilde{\alpha}_3\tilde{\tilde{\gamma}}\bar{p} \end{pmatrix}$$

Now

$$Y_2 = Y_1 + ({}^t\widetilde{l_2}(Y_R - Y_L))\widetilde{r_2}$$

and the last components of $\widetilde{r_2}$ are null, hence $u_1 = u_2$ and $p_1 = p_2$. The approximate solution is thus in agreement with the exact solution of the Riemann problem. Even more, if we assume that initial conditions agree with $\Delta u = 0$ and $\Delta p = 0$, the following holds $Y_1 = Y_L$ and $Y_2 = Y_R$ (see Reference [12]). This results in the fact that for some particular EOS such as perfect gas EOS and Tammann EOS, cell averages of velocity and pressure are perfectly preserved through the 2-wave, when focusing on single moving contact discontinuity and scheme VFRoe ncv (τ, u, p) (see Reference [14] and Appendix A.1 for a general expression of the EOS).

Another property of this scheme is that single 1-shocks (respectively, 3-shocks) are preserved in the sense that exact jump conditions and approximate jump conditions arising from linearized system are equivalent, when restricting to perfect gas EOS. In other words, if we set σ the speed of the shock wave and $[\alpha]$ the jump of α through this shock wave, then

$$-\sigma[W] + [F(W)] = 0$$

and

$$-\sigma[Y] + B(\overline{Y})[Y] = 0$$

are the same (see Reference [12] for more details). However, note that this scheme does not fulfil the Roe condition (see Reference [34]).

Eventually, we note that strictly speaking, the value $\tilde{\bar{\gamma}}$ is completely determined for a given choice of Y. Details concerning the discrete preservation of the positivity of density and pressure intermediate states can be found in Reference [12].

3.4. *VFRoe with non-conservative variable* (ρ, u, p)*—PVRS*

We now set $Y(W) = {}^t(\rho, u, p)$. This scheme actually identifies with the PVRS (primitive variable Riemann solver) scheme proposed by Toro, in Reference [16] or Reference [17]. Coefficients $\tilde{\alpha}_1$ and $\tilde{\alpha}_3$ are now

$$\tilde{\alpha}_1 = \frac{1}{2\tilde{c}^2}(-\bar{\rho}\tilde{c}\Delta u + \Delta p)$$

$$\tilde{\alpha}_3 = \frac{1}{2\tilde{c}^2}(\bar{\rho}\tilde{c}\Delta u + \Delta p)$$

Hence,

$$Y_1 = \begin{pmatrix} \rho_L + \tilde{\alpha}_1 \\ u_L - \tilde{\alpha}_1 \frac{\tilde{c}}{\bar{\rho}} \\ p_L + \tilde{\alpha}_1 \tilde{c}^2 \end{pmatrix} \quad \text{and} \quad Y_2 = \begin{pmatrix} \rho_R - \tilde{\alpha}_3 \\ u_R - \tilde{\alpha}_3 \frac{\tilde{c}}{\bar{\rho}} \\ p_R - \tilde{\alpha}_3 \tilde{c}^2 \end{pmatrix}$$

Once again, we check that

$$Y_2 = Y_1 + ({}^t\widetilde{l_2}(Y_R - Y_L))\widetilde{r_2}$$

so that the approximate intermediate states mimic the behaviour of the exact Godunov scheme. Moreover, for perfect gas EOS and Tamman EOS, cell averages of Riemann invariants of the 2-wave are perfectly preserved. The above-mentioned remark concerning jump conditions no longer holds, even when restricting to perfect gas EOS.

If we turn now to intermediate states of pressure, we note that PVRS scheme computes

$$p_1 = p_2 = \bar{p}\left(1 - \frac{\hat{\gamma}(\bar{p},\bar{\rho})\Delta u}{2\tilde{c}}\right)$$

Thus, the pressure intermediate states are strictly positive as soon as

$$\frac{\Delta u}{\tilde{c}} < \frac{2}{\hat{\gamma}(\bar{p},\bar{\rho})}$$

This should be compared with continuous condition for vacuum occurrence

$$\Delta u < X_{\mathrm{L}} + X_{\mathrm{R}} \tag{5}$$

where

$$X_i = \int_0^{\rho_i} \frac{c(\rho, s_i)}{\rho}\,\mathrm{d}\rho$$

where s_i denotes the specific entropy. Thus, if we restrict to some symmetrical double rarefaction wave with perfect gas EOS, we note that the upper bound of $\Delta u/\tilde{c}$ to avoid occurrence of vacuum is $4/(\gamma-1)$ in the 'continuous case' and $2/\gamma$ in the 'discrete case' for PVRS scheme. Using the standard value $\gamma = 1.4$ provides 10 and 10/7, respectively.

3.5. *VFRoe scheme with flux variable (VFFC)*

This corresponds to the choice: $Y(W) = F(W)$. This scheme VFFC was first introduced in Reference [8] (see also References [9, 10] for further details). The associated 1D Riemann problem is now

$$\frac{\partial F(W)}{\partial t} + A(\overline{W})\frac{\partial F(W)}{\partial x} = 0$$

$$F(W(x,0)) = \begin{cases} F_{\mathrm{L}} = F(W_{\mathrm{L}}) & \text{if } x < 0 \\ F_{\mathrm{R}} = F(W_{\mathrm{R}}) & \text{if } x > 0 \end{cases}$$

The interface numerical flux F^* is computed with the help of eigenstructure of the Jacobian matrix $A(\overline{W})$, as occurs when focusing on the basic VFRoe scheme.

3.6. *Rusanov scheme*

Unlike schemes presented above, Rusanov scheme do not solve an approximate Riemann problem at each interface (see Reference [18]). Numerical flux of Rusanov scheme is

$$\phi(W_{\mathrm{L}}, W_{\mathrm{R}}) = \frac{F(W_{\mathrm{L}}) + F(W_{\mathrm{R}})}{2} - \frac{1}{2}\lambda_{\mathrm{L,R}}^{\mathrm{MAX}}(W_{\mathrm{R}} - W_{\mathrm{L}})$$

with

$$\lambda_{\mathrm{L,R}}^{\mathrm{MAX}} = \max(|u_{\mathrm{L}}| + c_{\mathrm{L}}, |u_{\mathrm{R}}| + c_{\mathrm{R}})$$

The mean density remains positive as soon as the C.F.L. condition below holds (see Reference [19] for more details)

$$\max_{j\in\mathbb{Z}}(|u_j^n|+c_j^n)\Delta t\leqslant\Delta x$$

Note that a similar condition is exhibited in Reference [1] for the Rusanov scheme with a MUSCL reconstruction with minmod slope limiter [35].

3.7. *Energy relaxation method applied to VFRoe with non-conservative variable* (τ, u, p)

The energy relaxation method was introduced in Reference [20], and used in References [3, 21]. We refer to these references for further details, and only provide herein an algorithmic version to compute the flux ϕ, resolving the Riemann problem (3) for the Euler equations.

This requires introducing two additional variables γ_1 and ε_2 to the conservative ones. Coefficient γ_1 must fulfil the following conditions to reach convergence of the energy relaxation method

$$\gamma_1>\sup_{\rho,\varepsilon}\Gamma(\rho,\varepsilon)\quad\text{where }\Gamma(\rho,\varepsilon)=1+\frac{p_{,\varepsilon}}{\rho} \tag{6}$$

$$\gamma_1>\sup_{\rho,\varepsilon}\gamma(\rho,\varepsilon)\quad\text{where }\gamma(\rho,\varepsilon)=\frac{\rho}{p}p_{,\rho}+\frac{p_{,\varepsilon}}{\rho} \tag{7}$$

where $\varepsilon=E/\rho-\frac{1}{2}(\rho u)^2/\rho^2$ and p is computed using the real EOS (2).

Internal energy ε_2 is defined as follows:

$$\varepsilon_2=\frac{E}{\rho}-\frac{1}{2}\frac{(\rho u)^2}{\rho^2}-\frac{p}{(\gamma_1-1)\rho}$$

We may introduce

$$W_1(\rho,u,p)=\begin{pmatrix}\rho\\ \rho u\\ \frac{1}{2}\rho u^2+\dfrac{p}{\gamma_1-1}\end{pmatrix}$$

and

$$F_1(W_1(\rho,u,p))=\begin{pmatrix}\rho u\\ \rho u^2+p\\ u(\frac{1}{2}\rho u^2+\gamma_1\dfrac{p}{\gamma_1-1})\end{pmatrix}$$

The four governing equations are

$$\begin{aligned}\frac{\partial W_1}{\partial t}+\frac{\partial F_1(W_1)}{\partial x}&=0\\ (\rho\varepsilon_2)_{,t}+(\rho u\varepsilon_2)_{,x}&=0\end{aligned} \tag{8}$$

with the given initial condition

$$ {}^t(\rho, u, p, \varepsilon_2)(x,0) = \begin{cases} {}^t(\rho_L, u_L, p_L, \varepsilon_{2L}) & \text{if } x<0 \\ {}^t(\rho_R, u_R, p_R, \varepsilon_{2R}) & \text{if } x>0 \end{cases} \tag{9} $$

Thanks to these, one may compute the VFRoe-ncv numerical flux pertaining to the latter system which is a hyperbolic system with three distinct eigenvalues which are those of the Euler system. The numerical flux with three components relative to the mass, momentum and energy equations will eventually be defined as follows:

$$ \phi(W_L, W_R) = \begin{pmatrix} F^*_{1,1} \\ F^*_{1,2} \\ F^*_{1,3} + (\rho u \varepsilon_2)^* \end{pmatrix} $$

noting $F^*_1 = {}^t(F^*_{1,1}, F^*_{1,2}, F^*_{1,3})$.
Since we use the VFRoe ncv (τ, u, p) scheme to solve the four-equation system, we get

$$ \begin{aligned} (\rho u \varepsilon_2)^* &= \rho^* u^* \varepsilon_{2L} \quad \text{if } \bar{u}_{LR} > 0 \\ &= \rho^* u^* \varepsilon_{2R} \quad \text{if } \bar{u}_{LR} < 0 \end{aligned} $$

Since ε_2 is defined for each Riemann problem resolution, this variable is not continuous in time (a jump occurs at each time step).

4. NUMERICAL RESULTS

All test cases have been computed for all schemes, but we do not present here all results (see Reference [1], pp. 53–451). However, they are all discussed in the following with some figures to focus on problems in critical configurations. Let us note that VFRoe ncv (τ, u, p) scheme without entropy correction has been investigated too, in order to emphasize the influence of the energy relaxation method.

The following tests are performed using constant CFL number; however, CFL number slightly increases at the beginning of the computation, from $0,1$ to $0,4$ in $t \in [0; T_{MAX}/4]$. Initial conditions refer to different 1D Riemann problems. The regular mesh contains 100 nodes.

We present results pertaining to perfect gas, focusing first on qualitative behaviour and then on measurement of L^1 error norm of four distinct solutions. Afterwards, some qualitative results are discussed, related to the Tammann EOS. The configurations of these test cases are similar to perfect gas EOS. Eventually, two cases are presented using Van Der Waals EOS, in order to emphasize some numerical problems through the LD field.

Remark 1
Unless otherwise specified, the average of $\hat{\gamma}$ which is used in all test cases is the following: $0.5((\hat{\gamma})_L + (\hat{\gamma})_R)$. The main advantage of this proposal issuing from Reference [11] is that the mean Jacobian matrix has real eigenvalues, provided that initial states have. This is not

necessarily true for some non-convex EOS when applying for expected value, i.e.: $\tilde{\hat{\gamma}} = \hat{\gamma}(\overline{Y})$. However, potential drawbacks of the former approach will be discussed when necessary. This remark obviously holds for Tammann EOS and Van der Waals EOS, but not for perfect gas state law.

4.1. Perfect gas EOS—qualitative behaviour

Case 1.1: *Perfect gas EOS—sod shock tube*. A 1-rarefaction wave travels to the left and a 3-shock moves to the right end. The contact discontinuity is right going. This case is usually examined but does not provide much information on schemes since discrepancies can hardly be exhibited between all schemes involved herein. However, one can note that 'first-order' Rusanov scheme is a little bit more diffusive than others schemes.

Left state	Right state
$\rho_L = 1$	$\rho_R = 0,125$
$u_L = 0$	$u_R = 0$
$p_L = 10^5$	$p_R = 10^4$

$T_{MAX} = 6$ ms

Case 1.2: *Perfect gas EOS—supersonic 1-rarefaction wave*. The 1-rarefaction wave contains a sonic point. As a result, for VFRoe ncv schemes, a wrong shock wave may develop at the origin. This is corrected by introducing an entropy correction at sonic point, when focusing on the so-called first-order scheme. This is no longer compulsory when handling MUSCL-type reconstruction, which is usually combined with RK2 time integration in order to avoid loss of stability. Note that VFFC scheme without entropy correction also provides a non-entropic shock at sonic point, but this appears to be very small when compared with those arising with VFRoe ncv approach with 'physical' variables. Moreover, since the energy relaxation method is applied with VFRoe ncv (τ, u, p) without entropy correction, a small jump can be detected at the sonic point (which vanishes when the mesh is refined). Since the first-order Rusanov scheme is not based on a linearized Riemann solver, no problem appears at the sonic point. All second-order schemes behave in the same way.

Left state	Right state
$\rho_L = 1$	$\rho_R = 0,01$
$u_L = 0$	$u_R = 0$
$p_L = 10^5$	$p_R = 10^3$

$T_{MAX} = 5$ ms

Case 1.3: *Perfect gas EOS—double supersonic rarefaction wave*. This case enables to predict the behaviour of the scheme close to wall boundary conditions when applying the mirror technique. Two rarefaction waves are present in the solution when u_R is positive. Due to symmetrical initial conditions, the contact discontinuity is a ghost wave. We note that in this particular case VFFC scheme no longer provides a convergent solution since it blows up after a few time steps. Although intermediate states of VFRoe ncv scheme are no longer admissible (see Reference [12]) it however provides a convergent solution. As usual, Rusanov

scheme is more diffusive than other schemes, but it provides rather good results.

Left state	Right state
$\rho_L = 1$	$\rho_R = 1$
$u_L = -1200$	$u_R = 1200$
$p_L = 10^5$	$p_R = 10^5$

$T_{MAX} = 2$ ms

Case 1.4: *Perfect gas EOS—double subsonic shock wave*. This case is very similar to the previous one, but two shocks are now travelling to the left and to the right since u_R is negative. It corresponds to an inviscid impinging jet on a wall boundary. For supersonic double shock waves with very high initial kinetic energy, small oscillations may occur close to shocks, even when the CFL number is such that waves do not interact. A similar behaviour is observed when computing the case with the help of Godunov scheme. Second-order schemes create some oscillations, even in a subsonic configuration, except for Rusanov scheme.

Left state	Right state
$\rho_L = 1$	$\rho_R = 1$
$u_L = 300$	$u_R = -300$
$p_L = 10^5$	$p_R = 10^5$

$T_{MAX} = 5$ ms

Case 1.5: *Perfect gas EOS—stationary 1-shock wave*. This case is usually considered to evaluate the stability of the (expected) stationary 1-shock wave, especially when the scheme does not comply with Roe's condition. In all cases, no instability arises, and all schemes (except for the energy relaxation method which inserts two points in the stationary shock wave profile and Rusanov scheme which smears the wave) actually perfectly preserve the steadiness, whatever the order is.

Left state	Right state
$\rho_L = 3/4$	$\rho_R = 1$
$u_L = 4/3$	$u_R = 1$
$p_L = 2/3$	$p_R = 1$

$T_{MAX} = 100$ s

Case 1.6: *Perfect gas EOS—unsteady contact discontinuity*. This case is interesting since it enables to check whether the Riemann invariants of the 2-wave are preserved from a discrete point of view. This essentially depends on the scheme and the EOS (see Appendix A.1). All (first- and second-order) computed schemes preserve velocity and pressure exactly constant, whereas density jump at the contact discontinuity is smeared. Note that Rusanov scheme is once again more diffusive than schemes based on a linearized Riemann solver and the energy relaxation method.

Left state	Right state
$\rho_L = 1$	$\rho_R = 0, 1$
$u_L = 100$	$u_R = 100$
$p_L = 10^5$	$p_R = 10^5$

$T_{MAX} = 20$ ms

Case 1.7: *Perfect gas EOS—supersonic 1-rarefaction wave propagating over 'vacuum'*. This is one difficult test case for all schemes based on approximate Riemann solvers. Moreover, problems may appear due to the fact that computers have to handle round off errors. The analytical solution is close to a pure 1-rarefaction wave over vacuum, since the variations through the LD field and the 3-shock are not significant. Note that some variables are not defined in vacuum, namely velocity u or specific volume τ. Indeed, for the first-order framework, the energy relaxation method applied to VFRoe ncv (τ, u, p) without entropy correction blows up after few time steps. However, VFRoe ncv (τ, u, p) scheme with entropy correction provides good results, except in the vacuum area, where velocity profile becomes less accurate on coarse mesh. Other first-order schemes (PVRS, VFFC and Rusanov) provide slightly better profiles, even near vacuum. The second-order energy relaxation method and second-order VFRoe ncv (τ, u, p) scheme provide good results, though the problem on the velocity profile in the vacuum area remains unchanged. Other second-order schemes perform well.

Left state	Right state
$\rho_L = 1$	$\rho_R = 10^{-7}$
$u_L = 0$	$u_R = 0$
$p_L = 10^5$	$p_R = 10^{-2}$

$T_{MAX} = 1$ ms

Case 1.8: *Perfect gas EOS—double rarefaction wave with vacuum*. This one too is interesting, since the violation of condition $(\gamma - 1)(u_R - u_L) < 2(c_R + c_L)$ results in a vacuum occurrence on each side of the origin. Since this test case provides a double supersonic rarefaction wave, VFFC scheme cannot handle these initial conditions, whatever the order. The energy relaxation method applied to VFRoe ncv (τ, u, p) scheme without entropy correction blows up too, restricting to the first-order approximation. However, these two schemes perform well when handling MUSCL reconstruction with RK2 time integration. Moreover, first- or second-order PVRS, VFRoe and Rusanov schemes preserve density and pressure positivity in this test case and provide good results too (recall that Rusanov scheme maintains positivity of the density under a standard CFL-like condition).

Left state	Right state
$\rho_L = 1$	$\rho_R = 1$
$u_L = -3000$	$u_R = 3000$
$p_L = 10^5$	$p_R = 10^5$

$T_{MAX} = 1$ ms

4.2. Perfect gas EOS—quantitative behaviour

We compute here five test cases (unsteady contact discontinuity, double subsonic shock wave, double subsonic rarefaction wave, Sod shock tube, supersonic 1-rarefaction wave with 3-shock wave) with several meshes: 100, 300, 1000, 3000 and 10 000 nodes. Numerical rates of convergence of the L^1 error are measured and presented. Continuous lines refer to first-order schemes, whereas dotted lines refer to second-order schemes. All results have been obtained using a constant CFL number $\max_i(|u_i| + c_i)\Delta t/h = 0.5$. In order to provide a detailed analysis

of true convergence rate, we distinguish:

(i) smooth solutions ($\mathscr{C}^\infty$),
(ii) pure contact discontinuities,
(iii) pure shock waves,
(iv) rarefaction waves connected with constant states (solutions are not $\mathscr{C}^1$),
(v) shock tube test cases which involve several waves.

When focusing on solutions in $\mathscr{C}^\infty$, three-point schemes provide order of convergence close to 1 and five-point scheme (with an MUSCL reconstruction) provide rates close to 2. The reader is referred, for instance, to the work described in References [28, 29]. In the first reference above, unsteady solutions are simply given by $u(x,t)=(a_0x+b_0)/(t+t_0)$, $u(x,t)-2c(x,t)/(\gamma-1)=c_0$, $p(x,t)=(\rho(x,t))^\gamma$, which are basic solutions of Euler equations with perfect gas EOS in a one-dimensional framework, and indeed correspond to the inner part of a rarefaction wave. This enables to check that expected rate of convergence is achieved focusing either on first-order or second-order scheme. This classical result no longer holds when the solution involves rarefaction waves (which are only $\mathscr{C}^0$) or discontinuities such as shock waves or contact discontinuities, which is the case in all the next studied solutions. Therefore, one may expect that the speed of convergence (when Δx tends to 0 with constant CFL number) slows down. Measure of L^1 error norm is achieved for unknowns ρ, u and p since the latter two are not expected to vary through the contact discontinuity whatever the initial conditions are.

Case 2.1: *Perfect gas EOS—unsteady contact discontinuity*. We focus here on initial conditions from Case 1.6. Results presented herein have been obtained using VFRoe ncv (τ,u,p). This test aims at measuring the rate of convergence when the solution involves a pure contact discontinuity. Pertaining to first-order schemes, the rate is approximatively $\frac{1}{2}$ and the addition of the MUSCL reconstruction with a RK2 method leads to a rate around $\frac{2}{3}$ (see results of Figure 49).

This preliminary result is important since it enables to explain the differences between Cases 2.2–2.3 (where no jump of density occurs through the contact discontinuity due to symmetry) and Cases 2.4–2.5 which correspond to classical shock tube experiments.

Case 2.2: *Perfect gas EOS—double subsonic shock wave*. The initial conditions of this test case come from Case 1.4. The contact discontinuity is a 'ghost wave' (no variable jumps through this wave). This explains why the rate of convergence of the first-order schemes is slightly higher for density than in the following Cases 2.4–2.5. For all schemes, the rates of convergence for density variable are slightly higher with the first-order approximation than with the second-order approximation, though the error of the first-order schemes is more important. It may be explained by the occurrence of tiny oscillations on the intermediate state caused by the second-order schemes. Here, all rates are close to 1, for both first- and second-order schemes.

Case 2.3: *Perfect gas EOS—double subsonic rarefaction wave*. This concerns Case 1.3, except for the fact that the initial velocity is set to: $u_L=-300$. As a result, the double rarefaction wave is subsonic (hence, the VFFC scheme provides meaningful results). Although the solution of this test case is continuous, connections between rarefaction waves and intermediate states are not regular. Thus, rates of convergence equal to 1 for the 'first'-order schemes and equal to 2 for the 'second'-order schemes can hardly be expected. The above-mentioned remark concerning the density through the contact discontinuity holds. Nonetheless,

unlike in the previous case, the rate of convergence for ρ, u and p with first-order scheme is smaller than 1. This means that error located at the beginning and at the end of the rarefaction wave affects much the global error, at least on these 'coarse' meshes, which is in agreement with the description of local L^1 error in Reference [28]. The rates of convergence of second-order schemes are with no doubt very close to 1 for all variables. Note that the error associated with the Rusanov scheme is close to the error of other schemes.

We now turn to standard shock tube experiments which involve several waves with true variations of all components. We may expect thus that both u, p will converge with rate 1 when using the so-called second-order scheme, and also that density convergence rate will be close to $\frac{2}{3}$.

Case 2.4: *Perfect gas EOS—sod shock tube*. Initial conditions of this test case are the same as Case 1.1. We recall here that local L^1 error has been examined in detail in Reference [28], which confirmed that great part of the error was located not only close to the contact discontinuity and the 3-shock, but also at the beginning and the end of the 1-rarefaction wave. Although Rusanov scheme is less accurate (in terms of error) than other schemes, its rate of convergence is the same. We can note that the rate of convergence of velocity and pressure are the same and higher than the rate of convergence pertaining to density, owing to the contact discontinuity. As expected, the second-order schemes converge faster (the slope is close to 1 for velocity and pressure, and a little bit higher than $\frac{2}{3}$ for density).

Case 2.5: *Perfect gas EOS—supersonic 1-rarefaction wave*. This refers to Case 1.2. Although the solution of this test case is composed of the same set of waves, we can measure here the influence of entropy correction for the first-order schemes. The rates of convergence are the same as above for all schemes, except for the energy relaxation method. Indeed, the first-order approximation provides higher rates of convergence than in the Sod shock tube case. The true rate of convergence in L^1 norm is hidden by the error associated with the sonic point due to the parametric entropy correction (which is confirmed by experiments with Godunov scheme on shallow water equations).

To conclude, we emphasize that focusing on the Sod tube test, the loss of accuracy is mainly due to the contact discontinuity, since it has been seen that rates of convergence for rarefaction waves or shock waves are greater than rates of convergence provided for a contact discontinuity. Hence, the main numerical diffusion is located on contact discontinuities and poor rates of convergence when dealing with discontinuous solutions are, again, merely due to contact discontinuities.

4.3. Tammann EOS

As mentioned in Section 2.5.2, one may retrieve by a suitable change of variables the Euler equations with perfect gas EOS from the Euler equations with Tammann EOS. Hence, the vacuum with the Tamman EOS is $\rho = 0$ and $p + p_c = 0$ and the condition for vacuum occurrence (5) becomes

$$\Delta u < \frac{2}{\gamma_c - 1}(c_{\mathrm{L}} + c_{\mathrm{R}})$$

where $c^2 = \gamma_c(p + p_c)/\rho$.

However, this equivalence is only meaningful in the 'continuous' framework. Indeed, it no longer holds from a discrete point of view (except for PVRS and VFRoe ncv (τ, u, p)),

and numerical results computed with the Tammann EOS are slightly different from previous results, namely with the perfect gas state law.

Case 3.1: *Tammann EOS—subsonic shock tube*. This case is somewhat different from its counterpart with perfect gas EOS, and is based on initial conditions provided in Reference [15]. However, the numerical approximation behaves as its counterpart with perfect gas EOS: all schemes provide good results, and Rusanov scheme is more diffusive than the others.

Left state	Right state
$\rho_L = 1100$	$\rho_R = 1000$
$u_L = 500$	$u_R = 0$
$p_L = 5 \times 10^9$	$p_R = 10^5$

$$T_{MAX} = 0.6 \text{ ms}$$

Case 3.2: *Tammann EOS—sonic rarefaction wave*. Once again, initial conditions are those provided in the reference above. Note that the energy relaxation method (with the first-order approximation) completely smears the non-entropic shock caused by VFRoe ncv (τ, u, p). All VFRoe ncv schemes have the same behaviour, and the Rusanov scheme is still more diffusive (first order or second order). Figures provided by first-order schemes are presented (Figures 1–6).

Left state	Right state
$\rho_L = 10^3$	$\rho_R = 10^3$
$u_L = 2000$	$u_R = 2000$
$p_L = 5 \times 10^8$	$p_R = 10^6$

$$T_{MAX} = 8 \text{ ms}$$

Case 3.3: *Tammann EOS—double subsonic rarefaction wave*. This test case is the counterpart of Case 1.3. Note that vacuum (i.e. $\rho = 0,\ p + p_c = 0$) can occur within the subsonic range, though it does not appear in this test case. Except for first-order Rusanov scheme, all schemes compute a glitch (or a spike) at the interface (where the contact discontinuity is located) on the density.

Left state	Right state
$\rho_L = 10^3$	$\rho_R = 10^3$
$u_L = -300$	$u_R = 300$
$p_L = 10^9$	$p_R = 10^9$

$$T_{MAX} = 0,5 \text{ ms}$$

Case 3.4: *Tammann EOS—double subsonic shock wave*. The only difference between this test case and the case presented above is due to the sign of initial velocities. As a result, instead of rarefaction waves, the solution is composed of two shock waves and a ghost contact discontinuity. The same behaviour on the density can be noted, namely a glitch at the interface

(even with the first-order Rusanov scheme).

Left state	Right state
$\rho_L = 10^3$	$\rho_R = 10^3$
$u_L = 300$	$u_R = -300$
$p_L = 10^9$	$p_R = 10^9$

$T_{MAX} = 0,5$ ms

Case 3.5: *Tammann EOS—stationary 1-shock wave*. A very slight difference may be seen when the average value of $\hat{\gamma}$ is chosen as $0.5((\hat{\gamma})_L + (\hat{\gamma})_R)$ instead of $\tilde{\hat{\gamma}} = \hat{\gamma}(\overline{Y})$ when focusing on VFRoe ncv with variable (τ, u, p). The shock remains steady only if the latter choice is considered from a theoretical point of view, which is confirmed by computation. However, other VFRoe ncv schemes provide as accurate results. First- or second-order Rusanov scheme is very diffusive, and the energy relaxation method introduces three or two points in the shock profile, according to the order of approximation.

Left state	Right state
$\rho_L = 2.10^{-10}$	$\rho_R = u_R^{-1}$
$u_L = 5.10^9$	$u_R = [4\gamma_c/(\gamma_c + 1)]\, p_c + [(\gamma_c - 1)/(\gamma_c + 1)]5 \times 10^9$
$p_L = p_c$	$p_R = p_L + u_L - u_R$

$T_{MAX} = 10^{-9}$ s

Case 3.6: *Tammann EOS—unsteady contact discontinuity*. The results provided by all schemes are similar to those provided with the perfect gas EOS (see Case 1.6). Pressure and velocity are exactly preserved (see Appendix A.1), and the jump of density is smeared by all schemes (in particular by the Rusanov scheme).

Left state	Right state
$\rho_L = 10^3$	$\rho_R = 10^2$
$u_L = 10^3$	$u_R = 10^3$
$p_L = 10^8$	$p_R = 10^8$

$T_{MAX} = 2$ ms

Case 3.7: *Tammann EOS—rarefaction wave propagating over vacuum*. This test computes a 1-rarefaction wave with a sonic point. The 2-contact discontinuity and the 3-shock wave are not of significant importance, as in Case 1.7. We have used in the following the last two cases: $\tilde{\hat{\gamma}} = \hat{\gamma}(\overline{Y})$. In this case, only VFRoe ncv (τ, u, p) with RK2-MUSCL integration and (first- or second-order) Rusanov scheme enable computation (see Figures 7–8). Note that the standard choice $0.5((\hat{\gamma})_L + (\hat{\gamma})_R)$ results in a blow up of the computation. Initial conditions make all other schemes blow up. These behaviours confirm the discrete difference between perfect gas EOS and Tammann EOS.

Left state	Right state
$\rho_L = 10^3$	$\rho_R = 10^{-9}$
$u_L = 0$	$u_R = 0$
$p_L = 10^8$	$p_R + p_c = 10^{-2}$

$T_{MAX} = 0,6$ ms

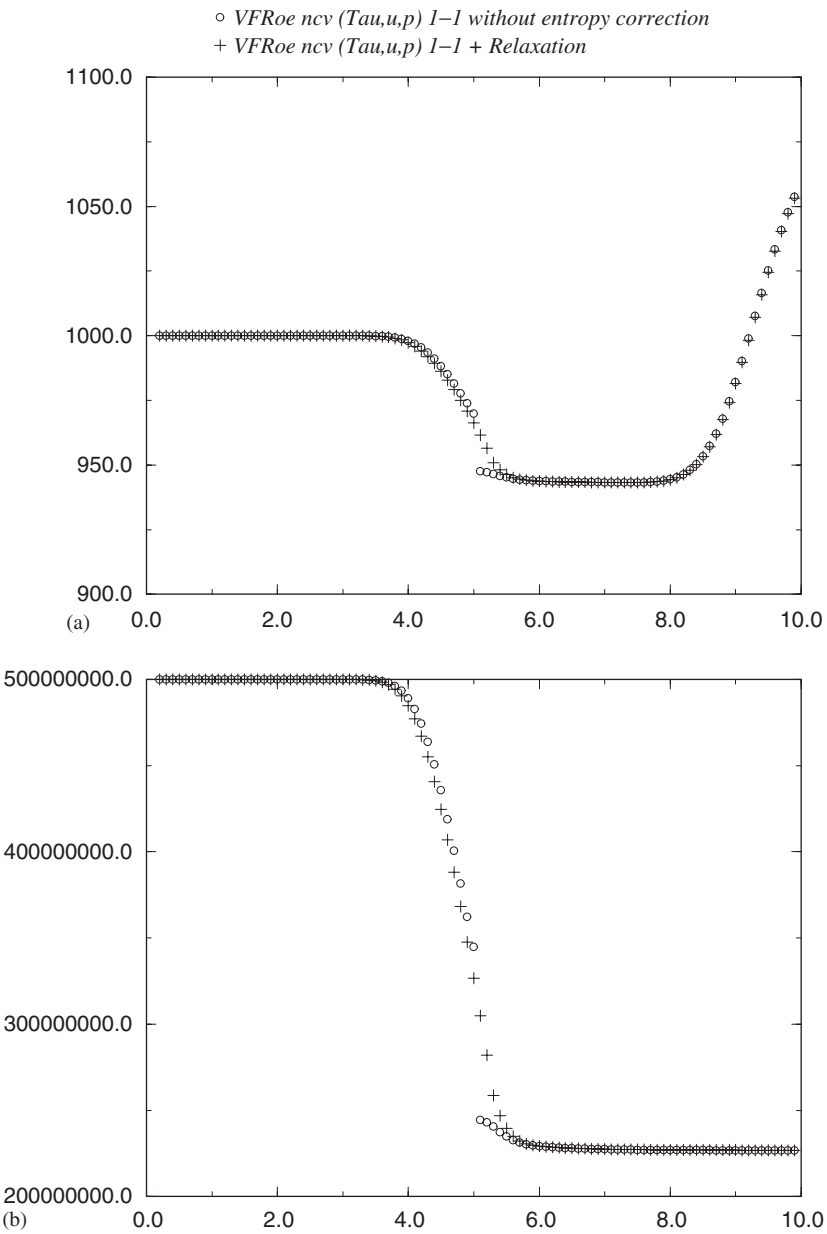

Figure 1. Case 3.2: density (a), $p + p_c$ (b).

Case 3.8: *Tammann EOS—vacuum occurrence*. This test results like Case 1.8 in a vacuum occurrence in the intermediate state. Recall that vacuum can appear though rarefaction waves are not supersonic. As above, VFRoe ncv (τ, u, p) and Rusanov schemes enable computation. Note that PVRS and VFRoe schemes also perform well in

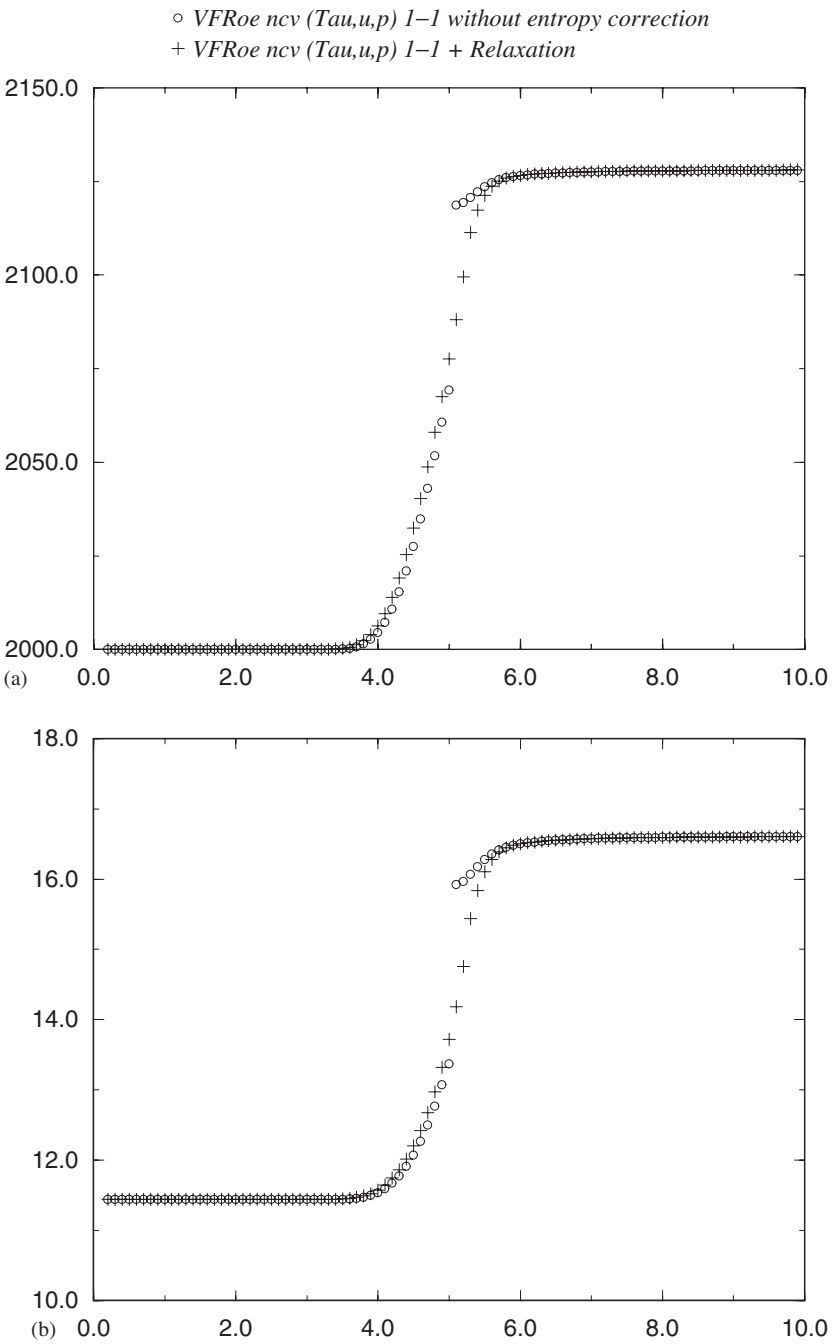

Figure 2. Case 3.2: velocity (a), $\hat{\gamma}(p,\rho)$ (b).

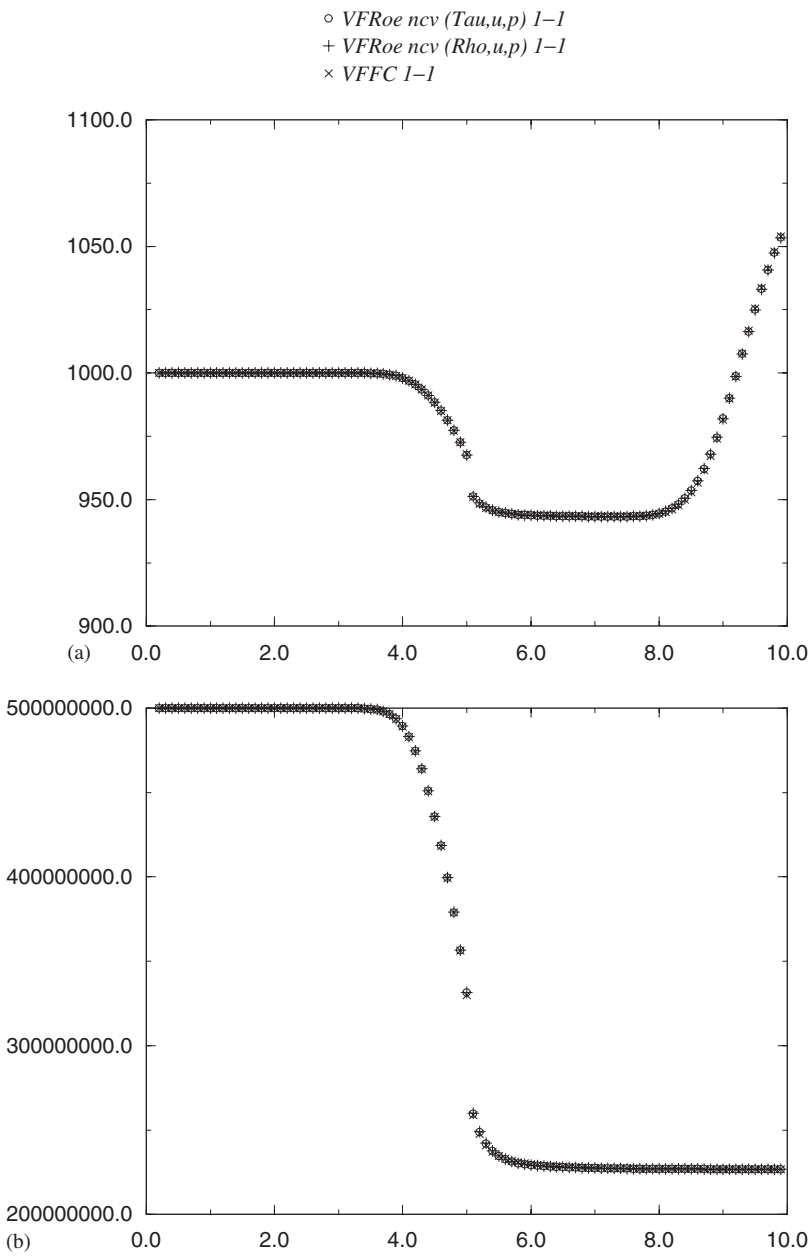

Figure 3. Case 3.2: density (a), $p + p_c$ (b).

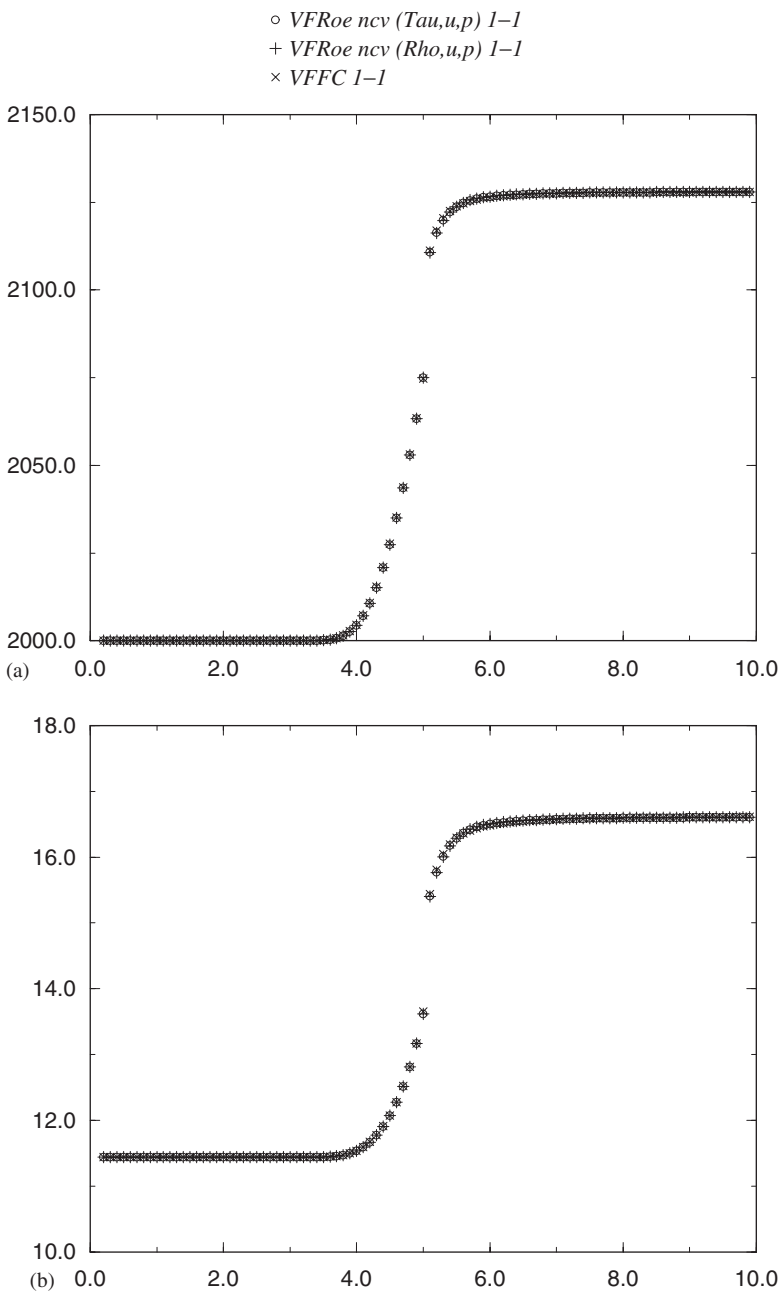

Figure 4. Case 3.2: velocity (a), $\hat{\gamma}(p,\rho)$ (b).

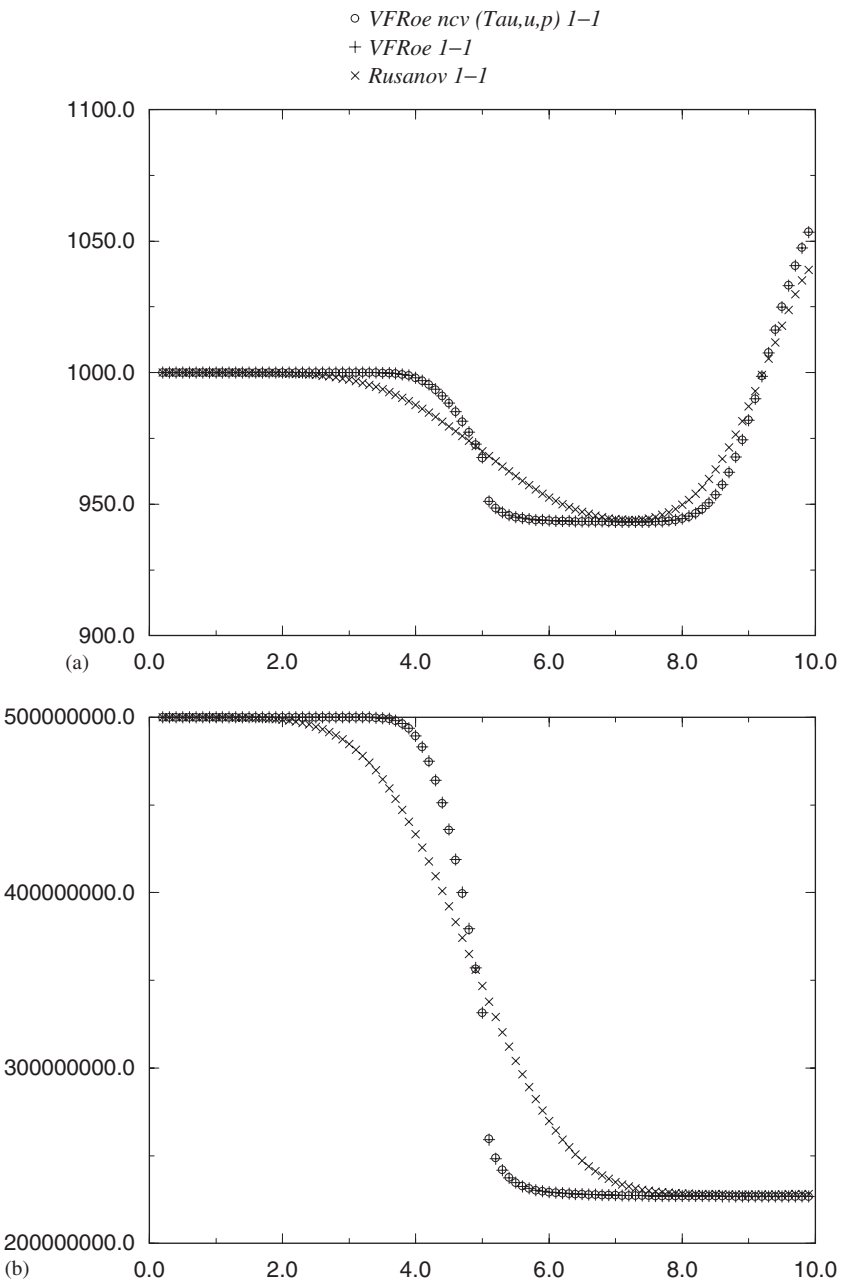

Figure 5. Case 3.2: density (a), $p + p_c$ (b).

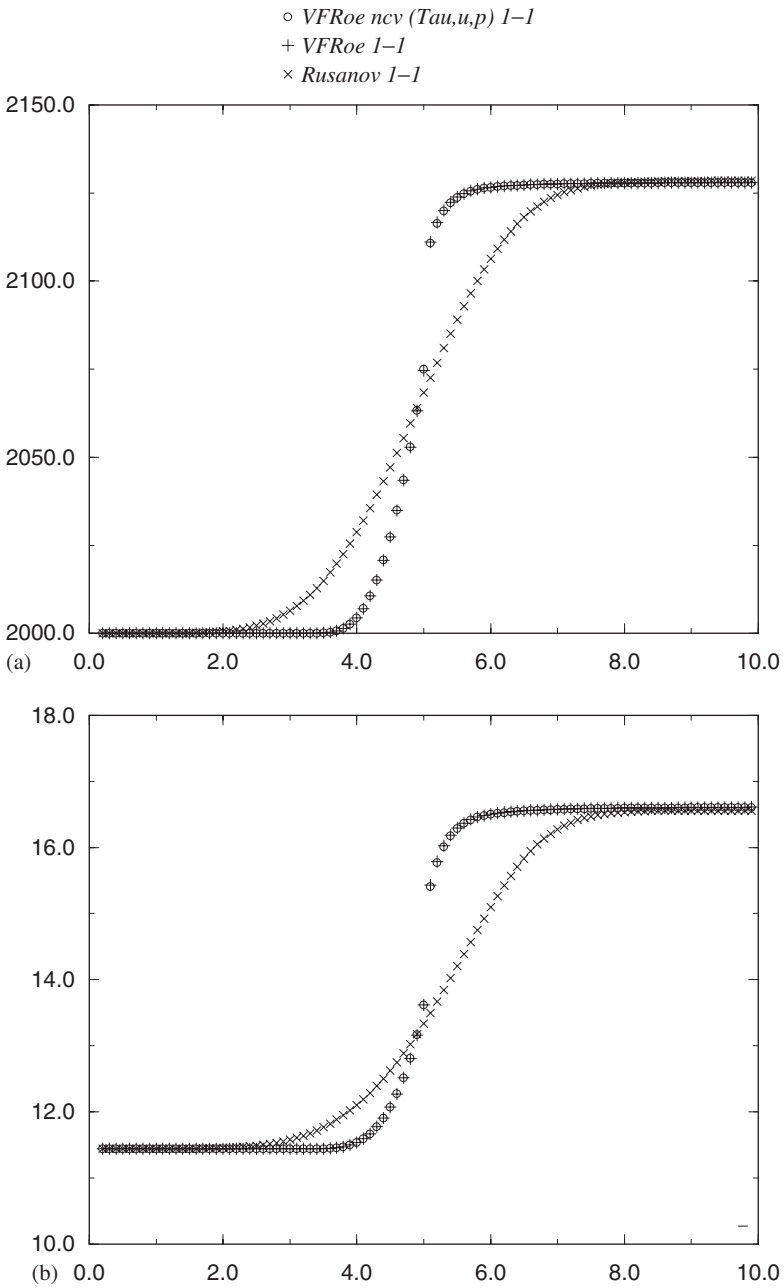

Figure 6. Case 3.2: velocity (a), $\hat{\gamma}(p,\rho)$ (b).

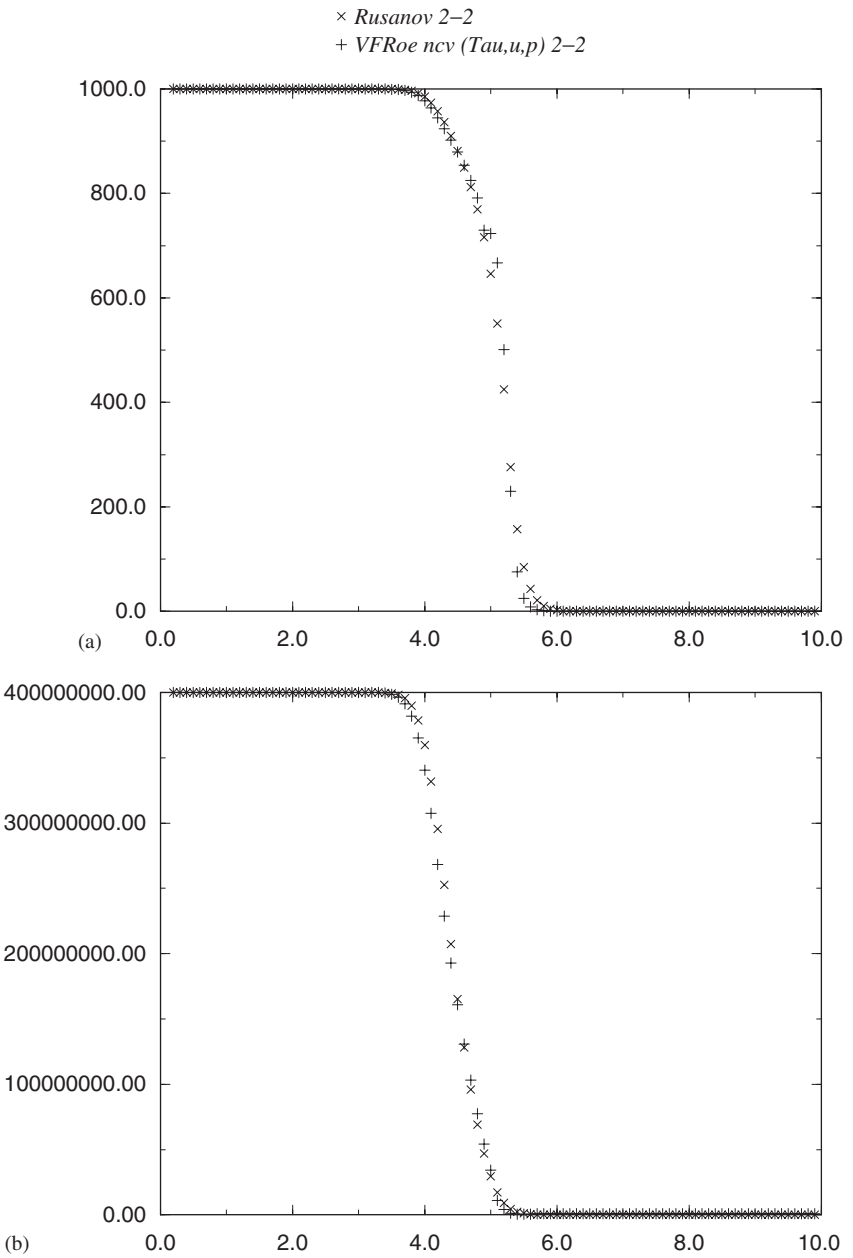

Figure 7. Case 3.7: density (a), $p + p_c$ (b).

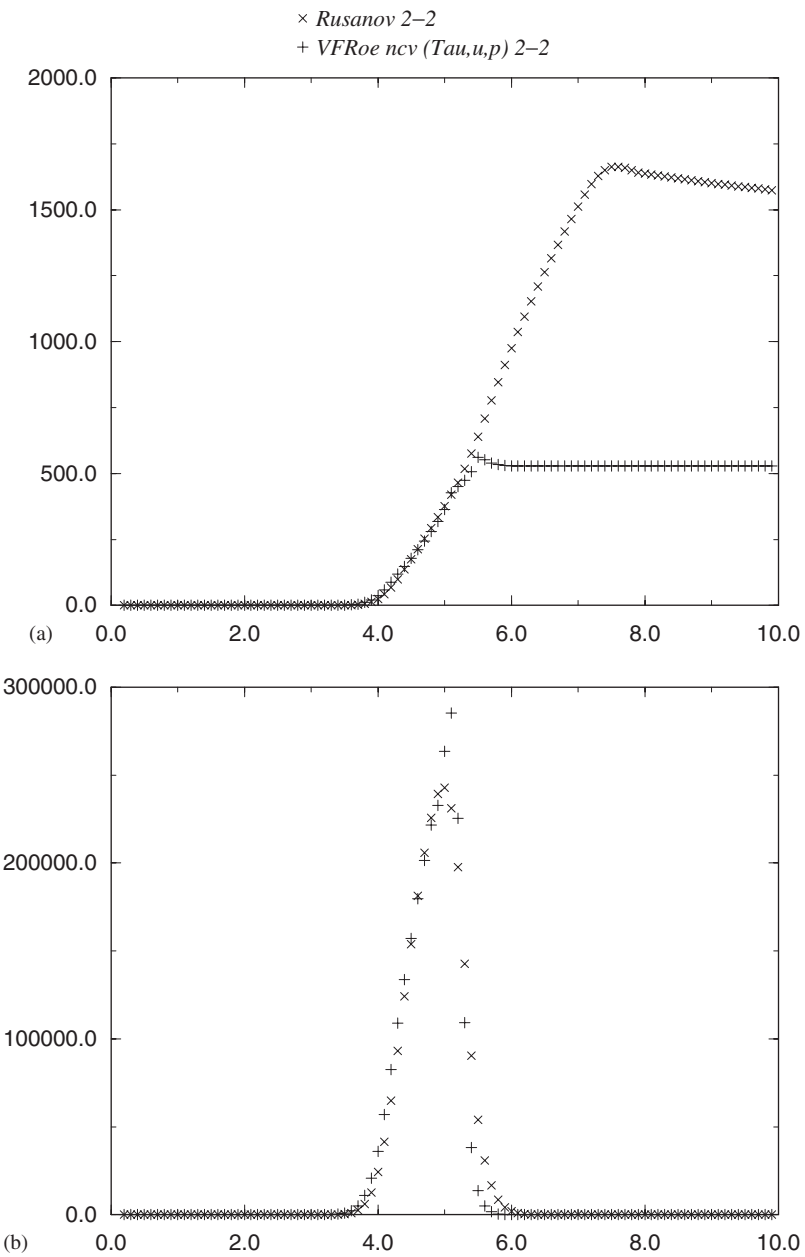

Figure 8. Case 3.7: velocity (a), momentum (b).

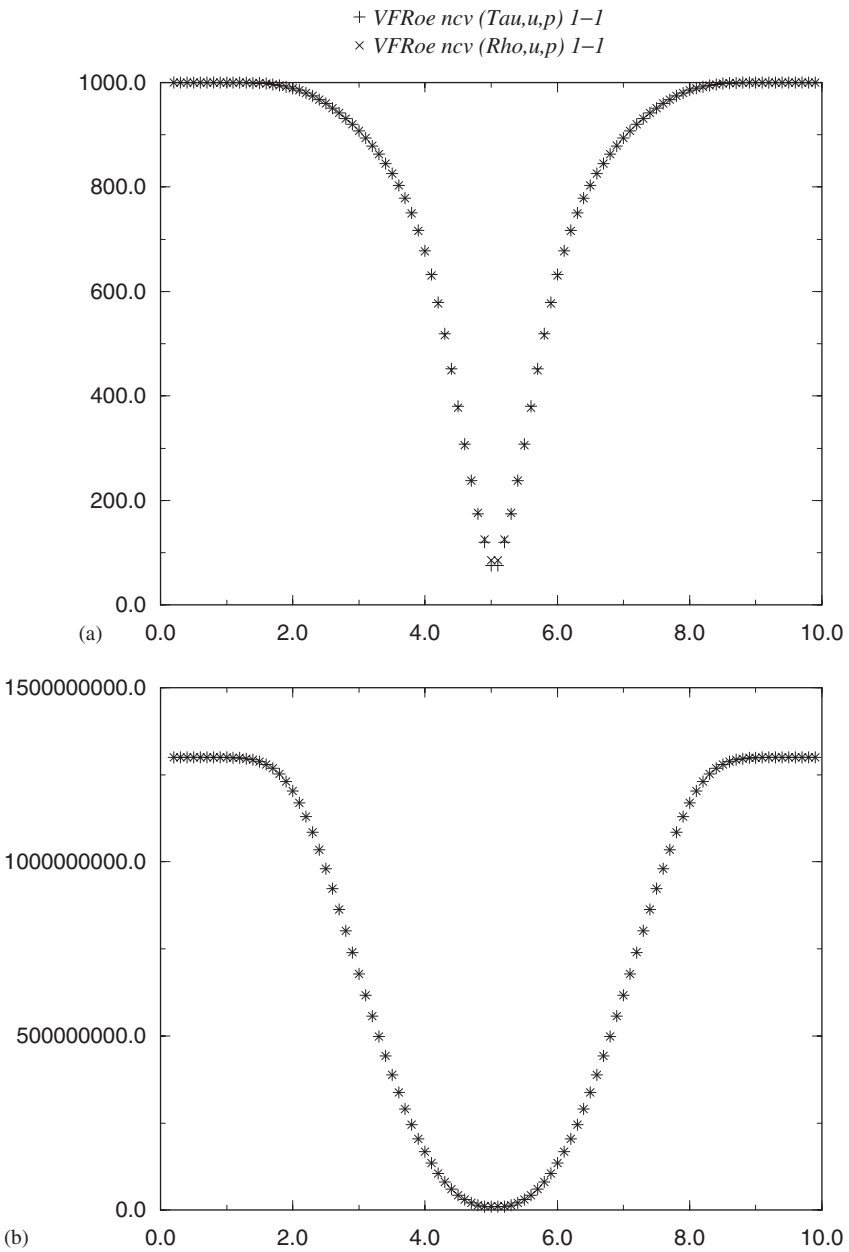

Figure 9. Case 3.8: density (a), $p + p_c$ (b).

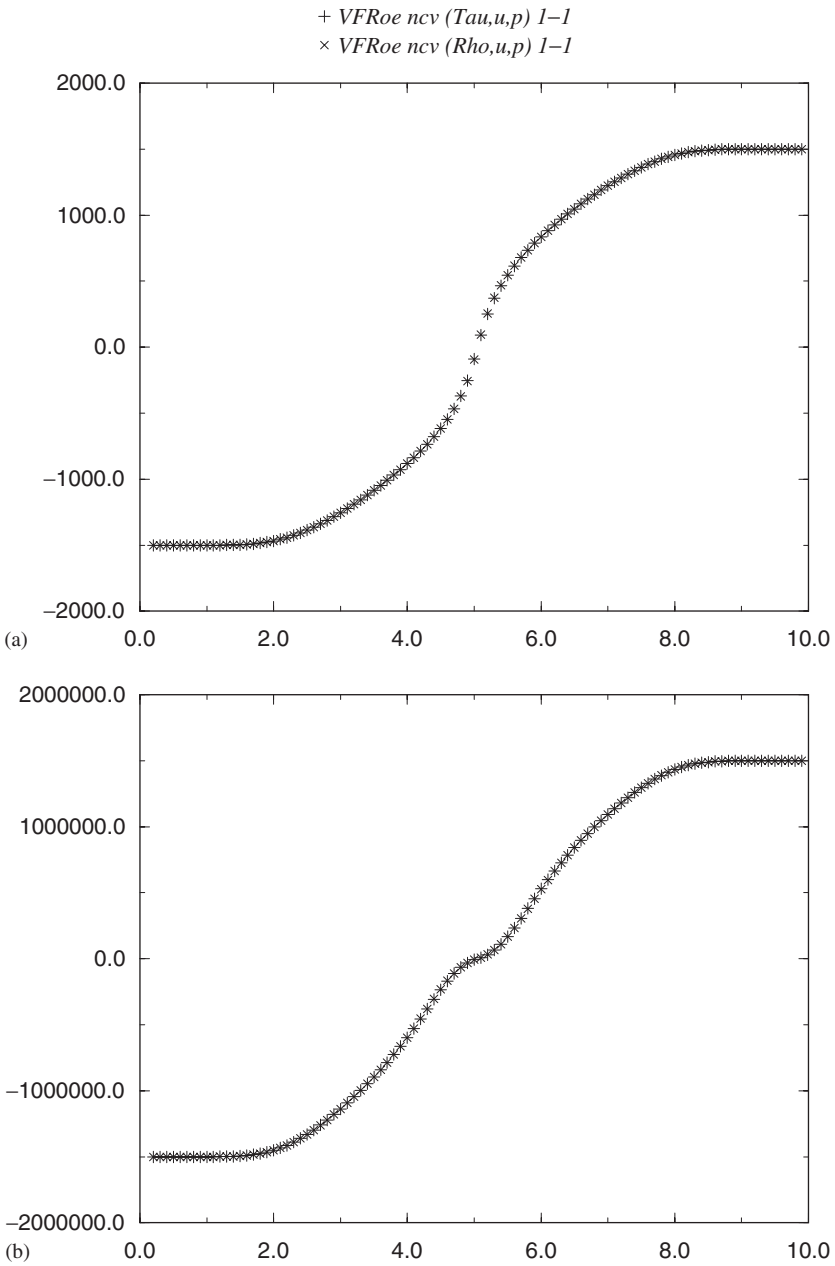

Figure 10. Case 3.8: velocity (a), momentum (b).

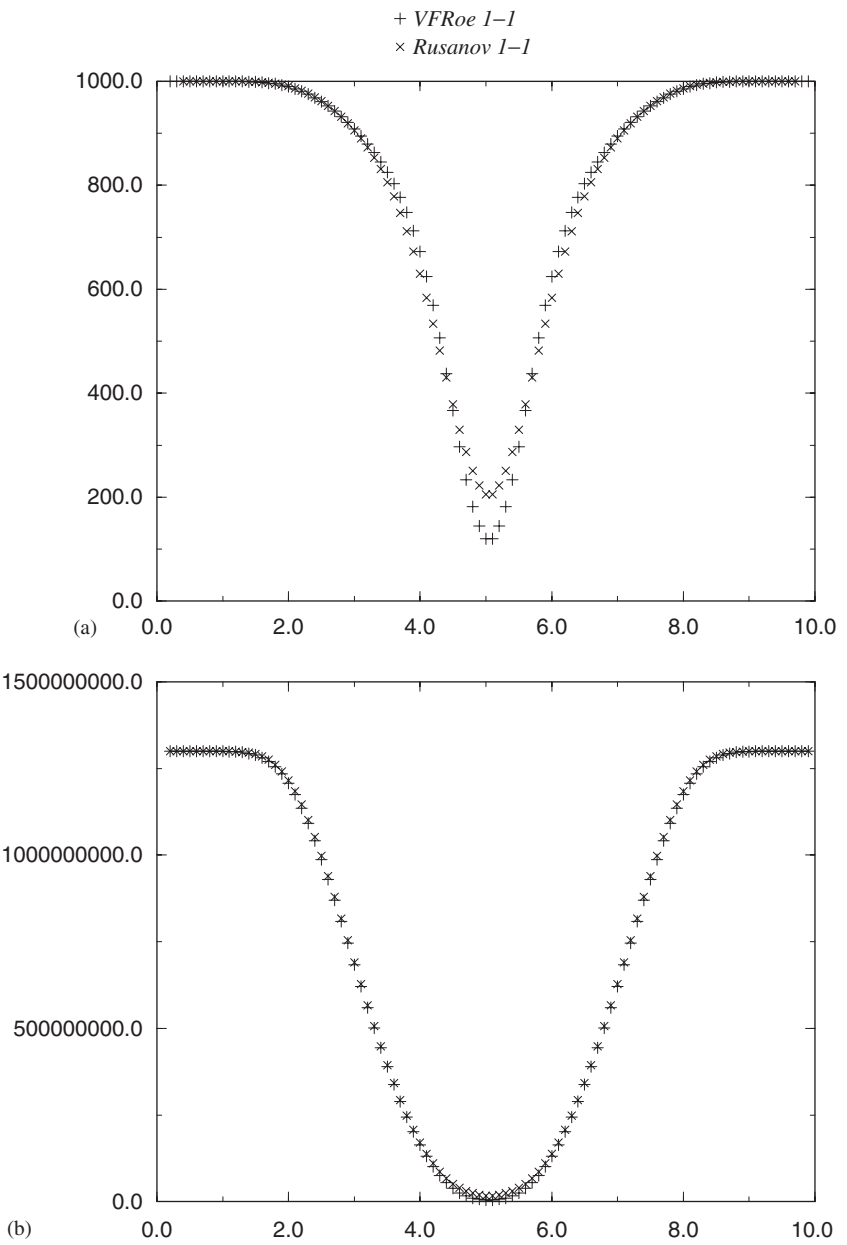

Figure 11. Case 3.8: density (a), $p + p_c$ (b).

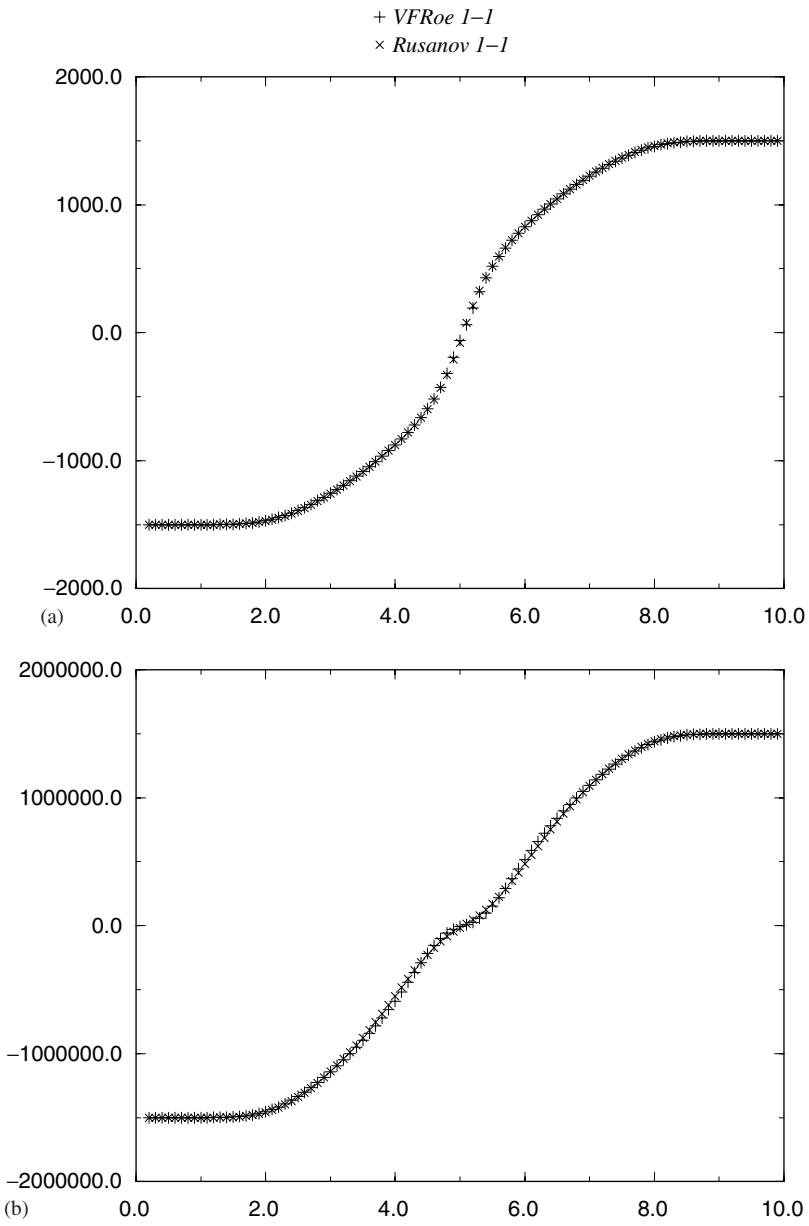

Figure 12. Case 3.8: velocity (a), momentum (b).

this test (see Figures 9–12).

Left State	Right state
$\rho_L = 10^3$	$\rho_R = 10^3$
$u_L = 1500$	$u_R = 1500$
$p_L = 10^9$	$p_R = 10^9$

$T_{MAX} = 0,6$ ms

4.4. Van Der Waals EOS

Results of both computations discussed below were achieved using the standard definition for VFRoe ncv (τ, u, p) and PVRS schemes and the mean of $\hat{\gamma}: 0.5((\hat{\gamma})_L + (\hat{\gamma})_R)$ instead of: $\tilde{\hat{\gamma}} = \hat{\gamma}(\overline{Y})$ when focusing on VFRoe ncv scheme. Differences between results for both choices could hardly be noticed for the following.

Case 4.1: *Van Der Waals EOS—subsonic 1-rarefaction wave*. Initial conditions below are taken from the paper by Letellier and Forestier [26]. The main advantage of this case is that it clearly exhibits the rather unpleasant behaviour around the contact discontinuity. Although both the exact Godunov scheme and VFRoe scheme with (τ, u, p) variables predict equal velocity and pressure of intermediate states on each side of the LD field, cell values of both u and p are not in equilibrium (this confirms results of Appendix A.1 for the VFRoe schemes with (φ, u, p) variable). Obviously, this well-known drawback (see Reference [26]) tends to vanish when the mesh size decreases, or when time increases. First-order results are provided in Figures 13–18.

Left state	Right state
$\rho_L = 333,33$	$\rho_R = 111,11$
$u_L = 0$	$u_R = 0$
$p_L = 37\,311\,358$	$p_R = 21\,770\,768$

$T_{MAX} = 5$ ms

Case 4.2: *Van Der Waals EOS—moving contact discontinuity*. Initial conditions are similar to those given in Case 1.6. Note that the Riemann invariants u and p are not very well preserved around the contact discontinuity when using coarse meshes, and 'first'-order scheme (see Appendix A.1 for more details on VFRoe ncv schemes with (φ, u, p) variable). The 'second'-order version of the scheme performs much better. Unlike sometimes heard, we emphasize that the approximation is still convergent. Small oscillations apart from the LD scheme which were reported in Reference [26] do not arise when using approximate Godunov schemes, which is still unexplained and rather amazing. Due to the very small rate of convergence measured in the LD field (smaller than $\frac{2}{3}$), it is clear that this slows down the whole rate of convergence on both velocity and pressure variable, compared with what happens when focusing on perfect gas EOS. Hence, none of the schemes presented here are able to preserve velocity and pressure constant on a given mesh (see Figures 19–24

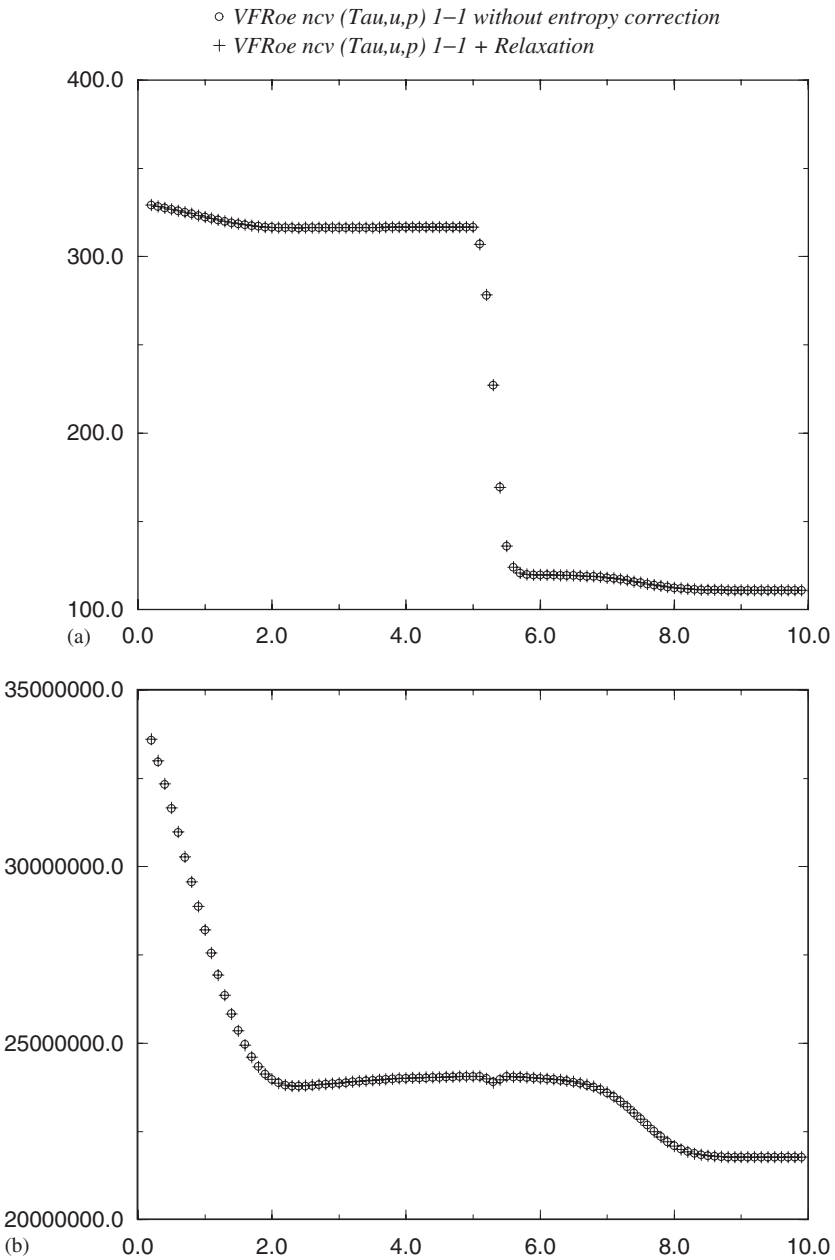

Figure 13. Case 4.1: density (a), $p + p_c$ (b).

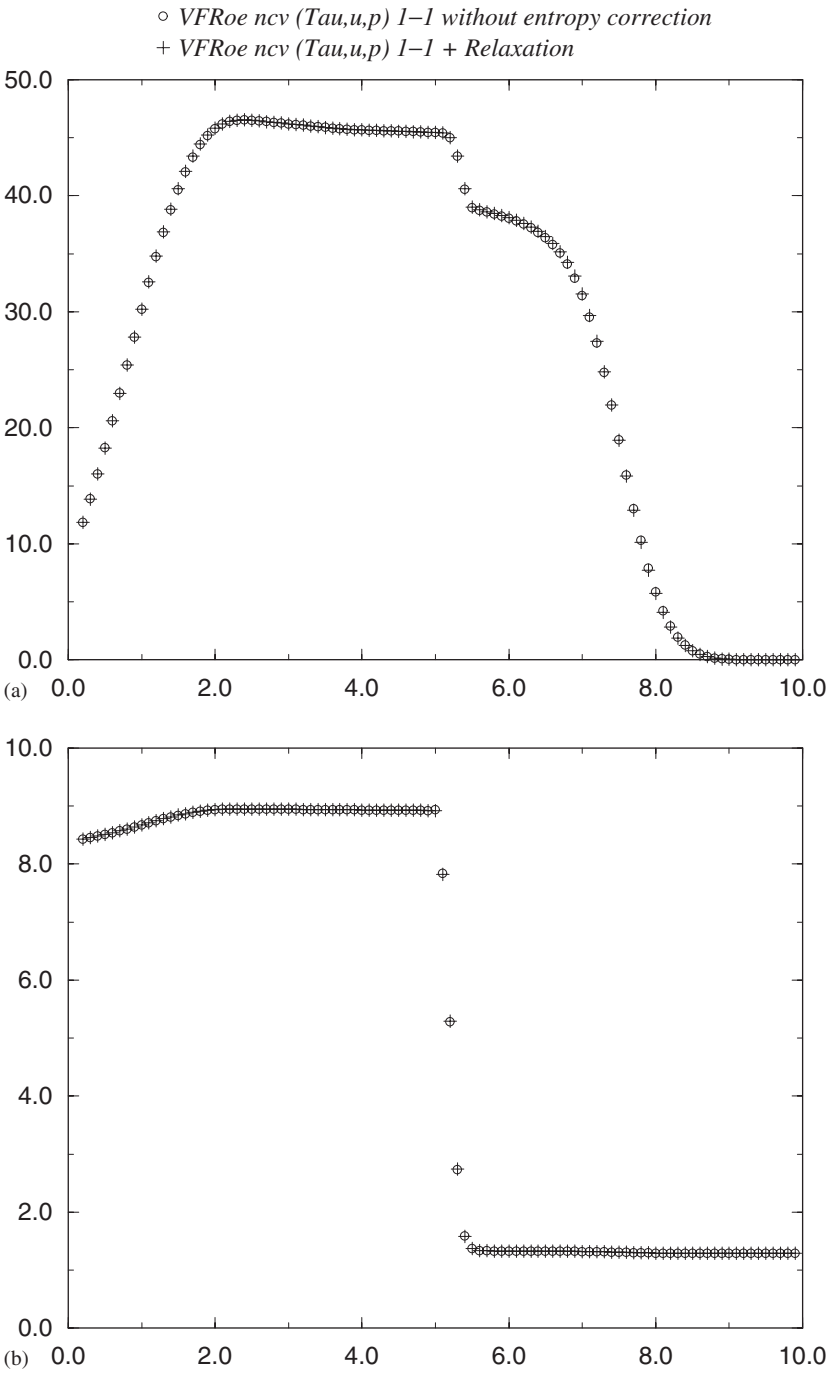

Figure 14. Case 4.1: velocity (a), $\hat{\gamma}(p,\rho)$ (b).

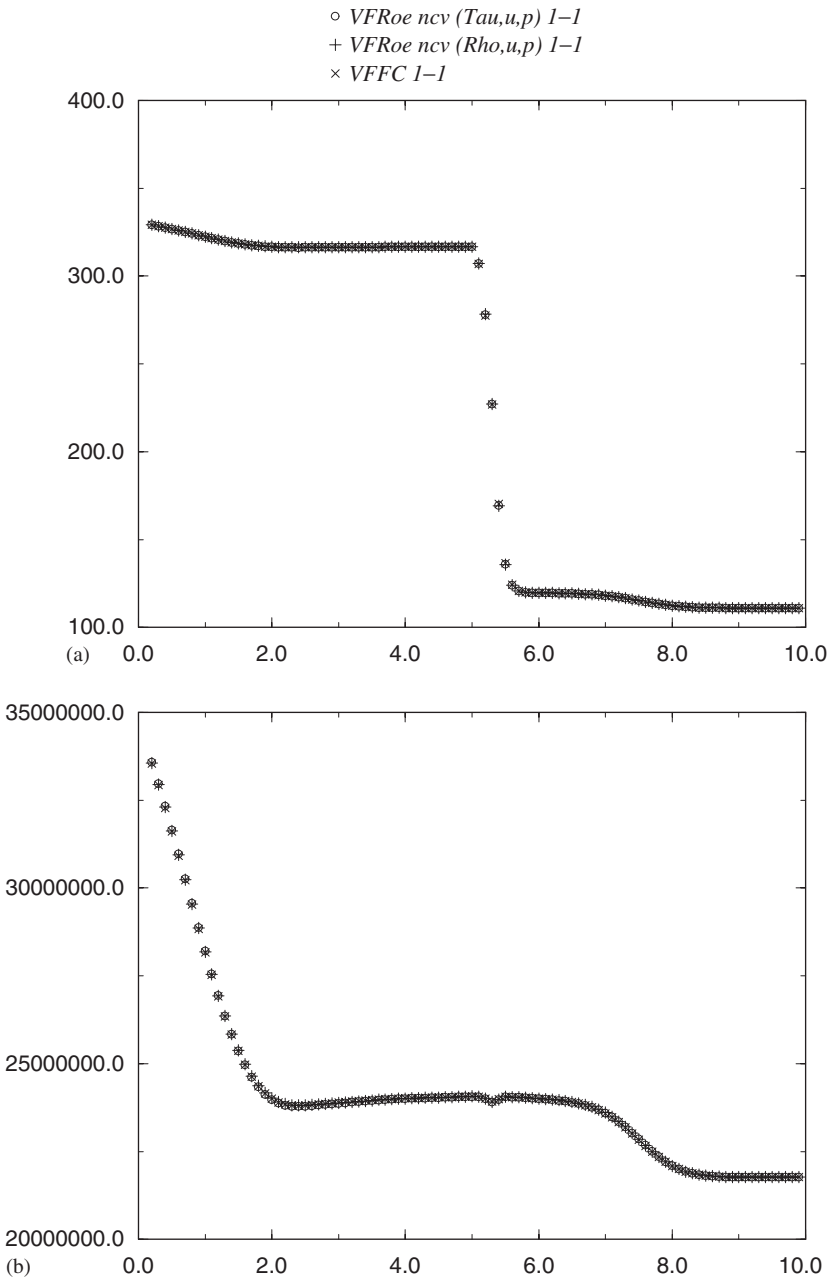

Figure 15. Case 4.1: density (a), $p + p_c$ (b).

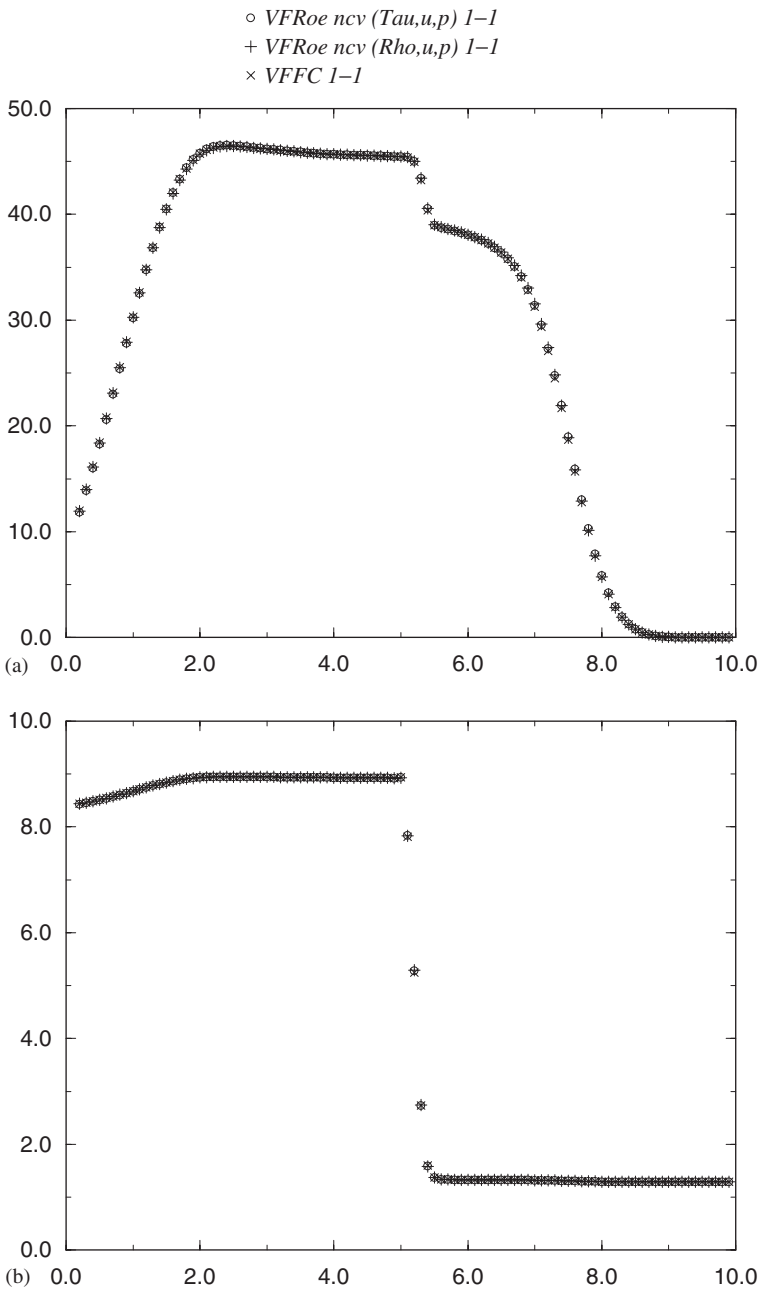

Figure 16. Case 4.1: velocity (a), $\hat{\gamma}(p, \rho)$ (b).

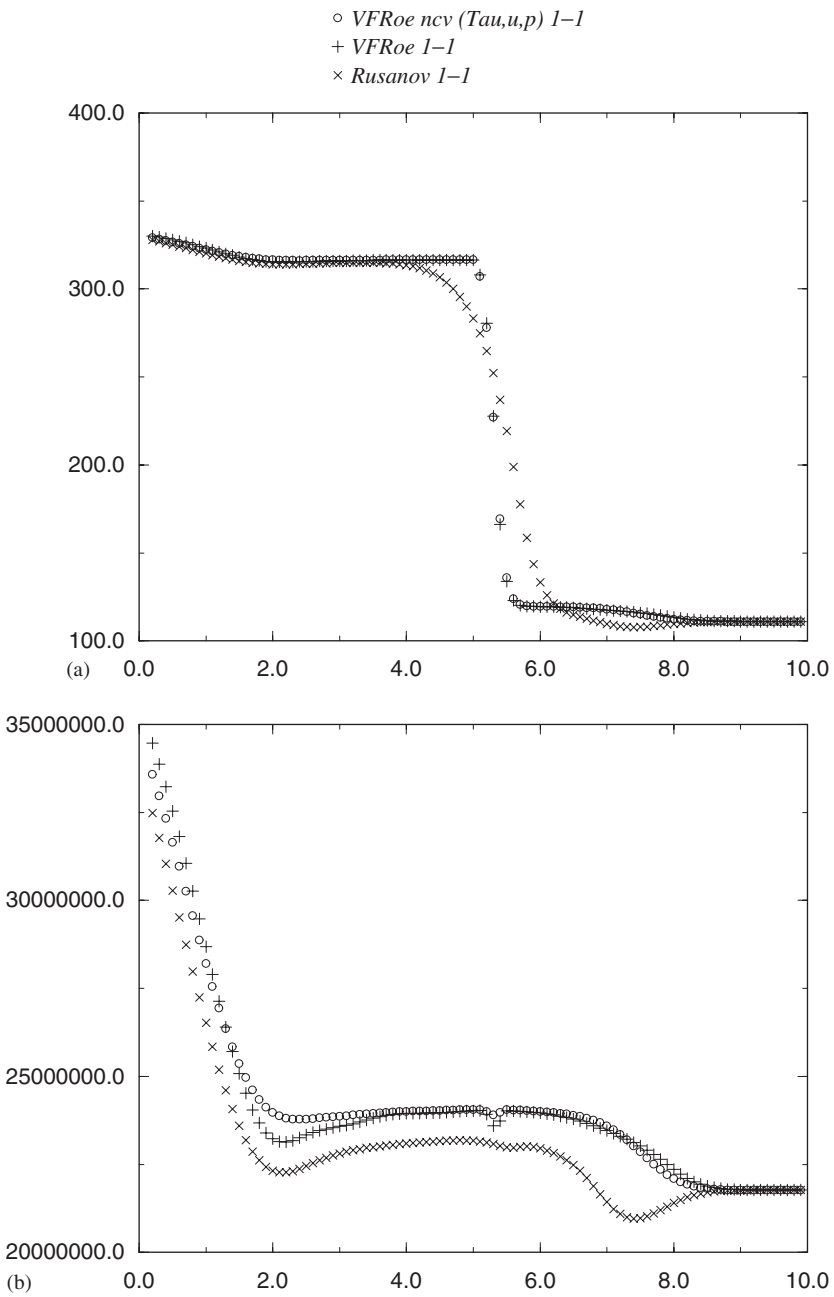

Figure 17. Case 4.1: density (a), $p + p_c$ (b).

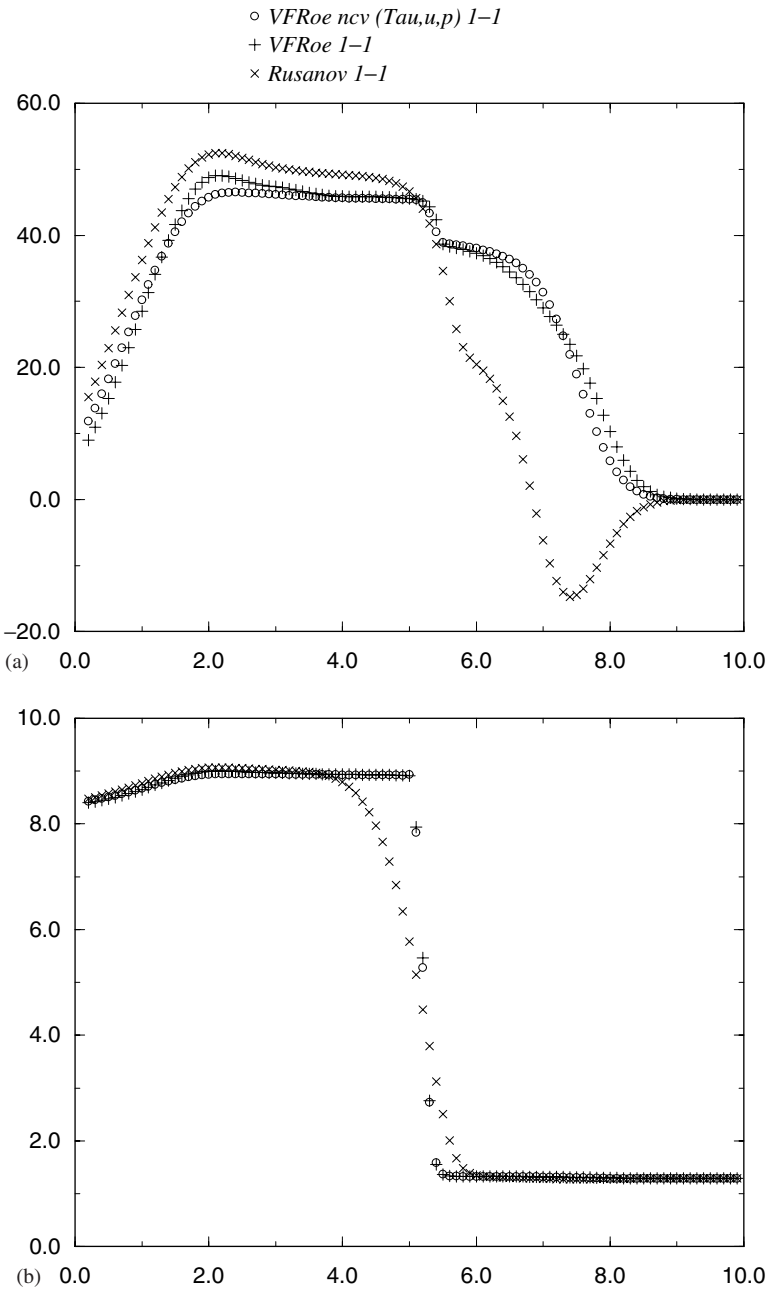

Figure 18. Case 4.1: velocity (a), $\hat{\gamma}(p,\rho)$ (b).

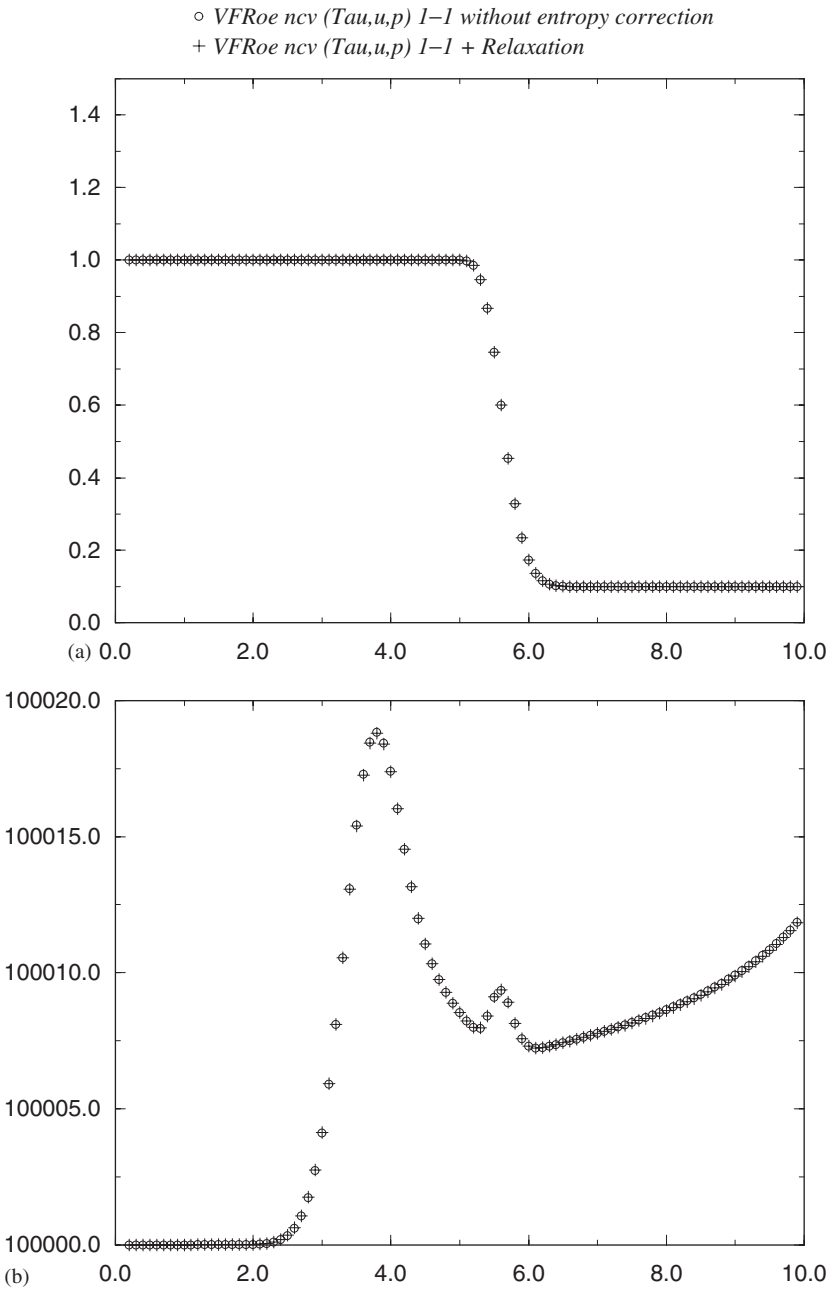

Figure 19. Case 4.2: density (a), $p + p_c$ (b).

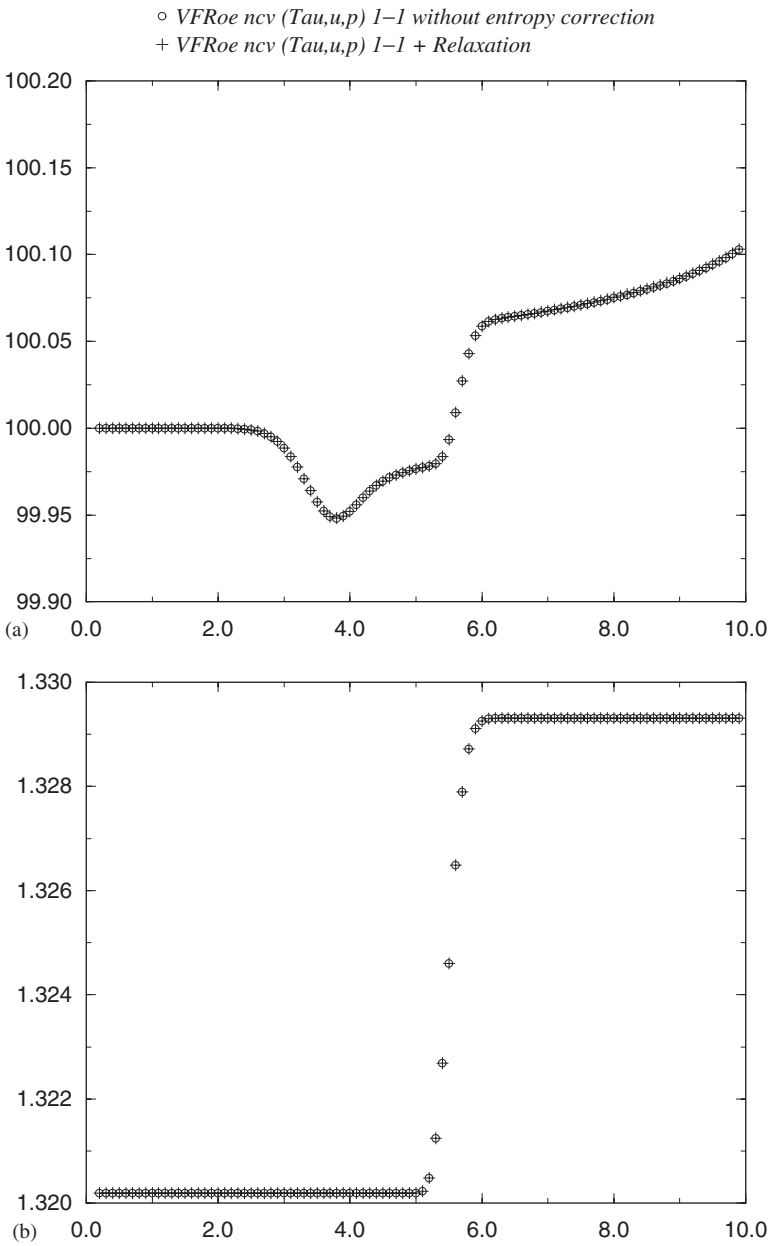

Figure 20. Case 4.2: velocity (a), $\hat{\gamma}(p, \rho)$ (b).

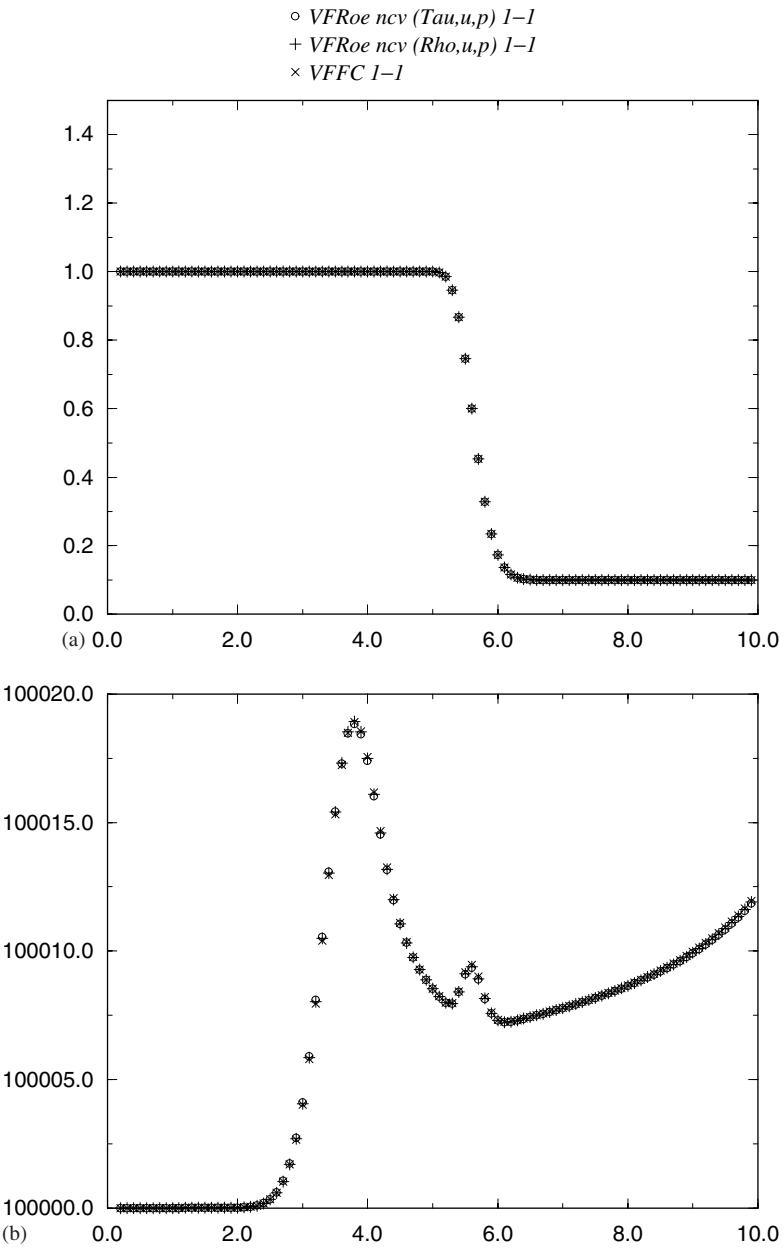

Figure 21. Case 4.2: density (a), $p + p_c$ (b).

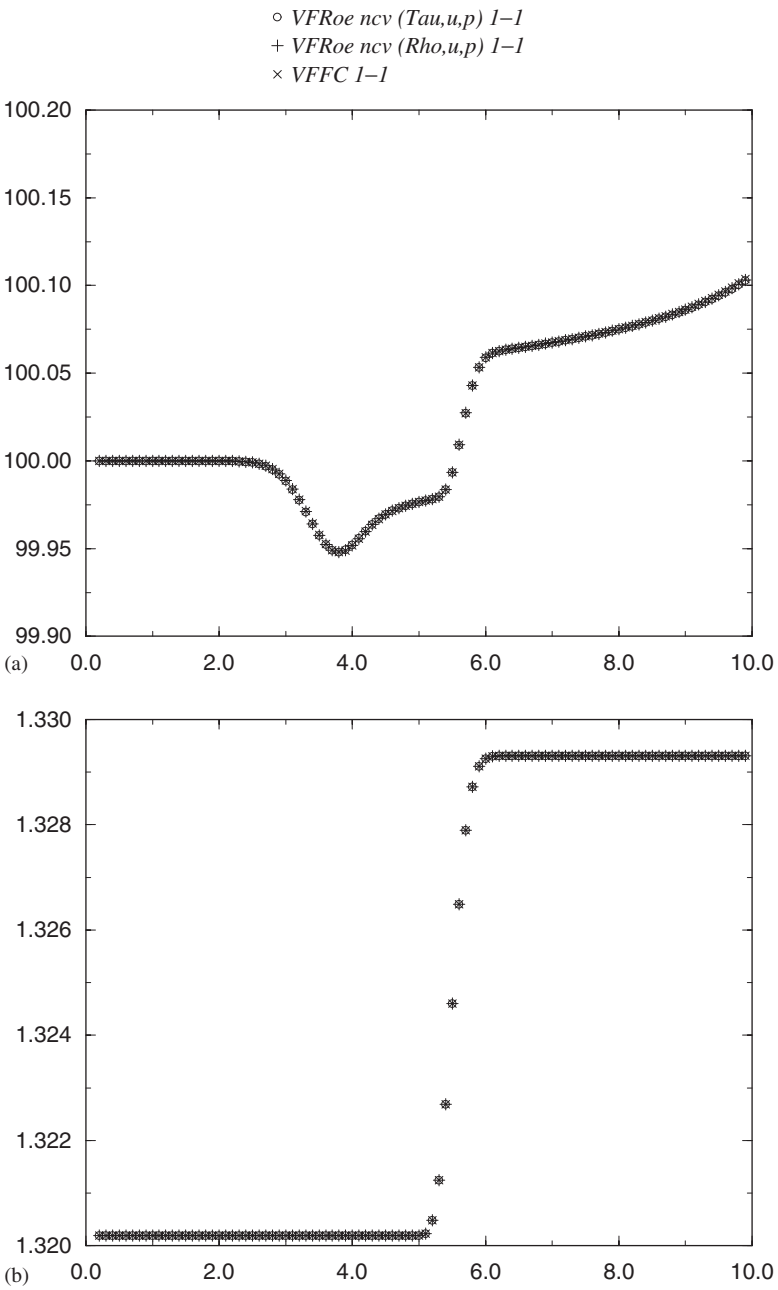

Figure 22. Case 4.2: velocity (a), $\hat{\gamma}(p,\rho)$ (b).

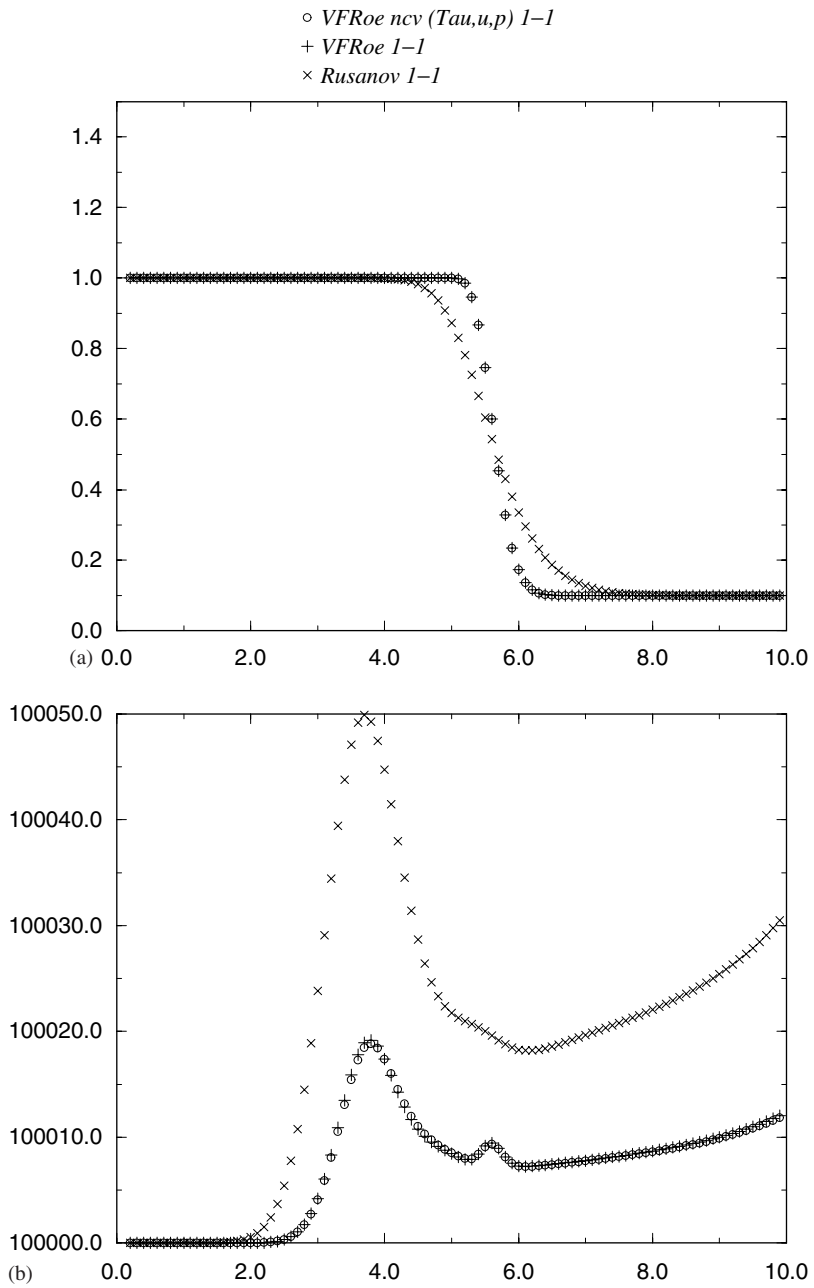

Figure 23. Case 4.2: density (a), $p + p_c$ (b).

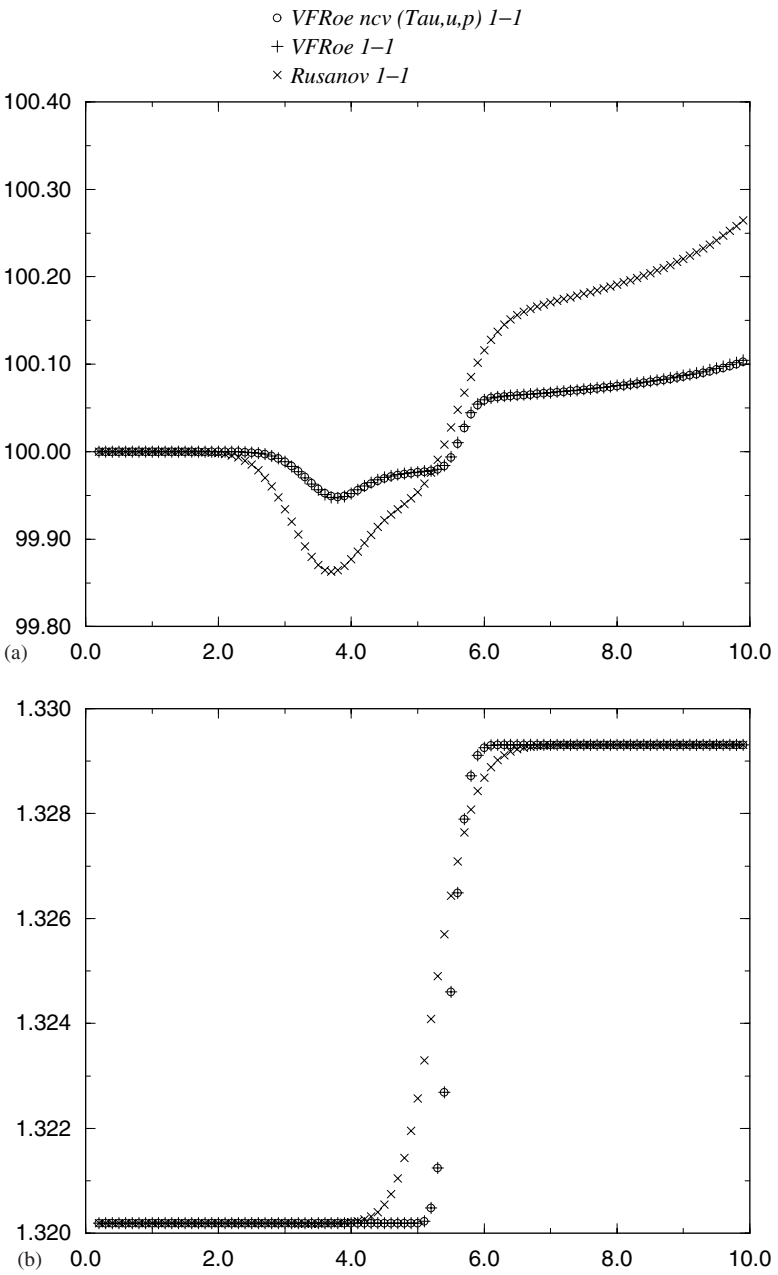

Figure 24. Case 4.2: velocity (a), $\hat{\gamma}(p,\rho)$ (b).

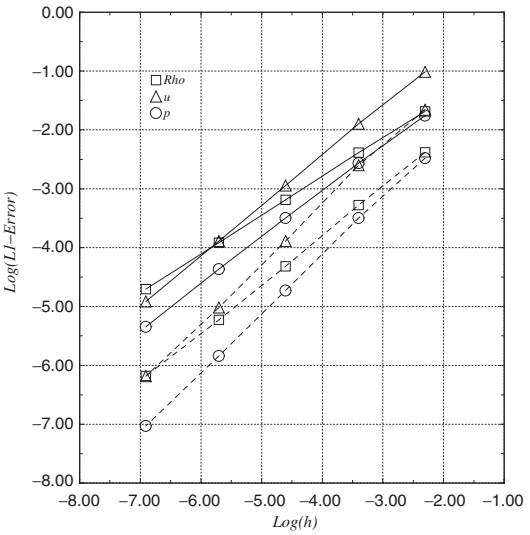

Figure 25. Energy relaxation.

for results performed by first-order schemes).

Left state	Right state
$\rho_L = 1$	$\rho_R = 10$
$u_L = 100$	$u_R = 100$
$p_L = 10^5$	$p_R = 10^5$

$T_{MAX} = 6$ ms

4.5. *Actual rates of convergence*

Perfect gas EOS—sod shock tube (Figures 25–30):

- Energy relaxation

	First order	Second order
ρ	0.654	0.791
u	0.853	0.967
p	0.812	0.988

- Rusanov

	First order	Second order
ρ	0.651	0.780
u	0.842	0.970
p	0.823	0.989

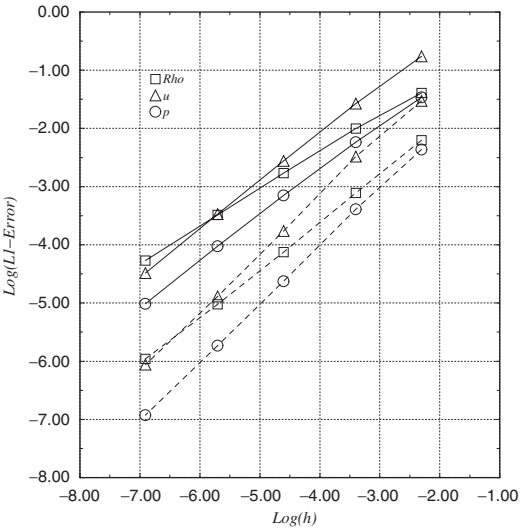

Figure 26. Rusanov.

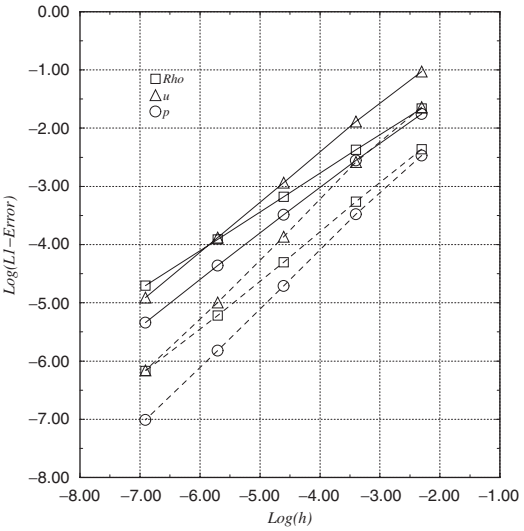

Figure 27. VFFC.

- VFFC

	First order	Second order
ρ	0.655	0.792
u	0.855	0.968
p	0.814	0.988

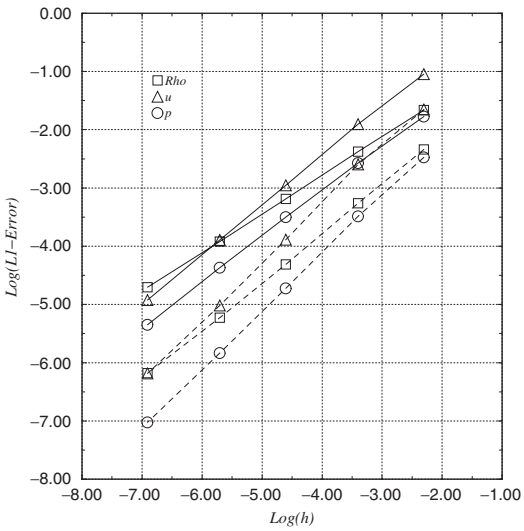

Figure 28. VFRoe.

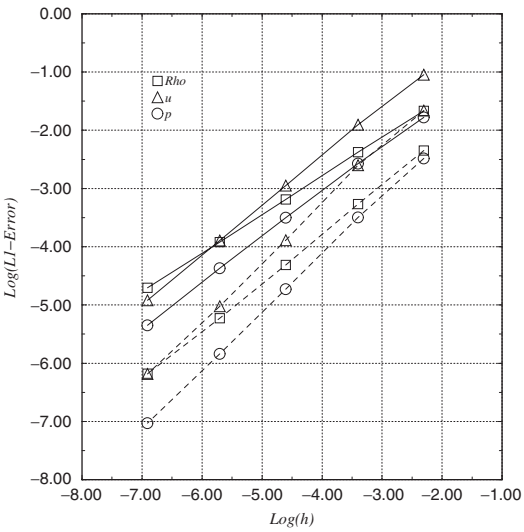

Figure 29. VFRoe ncv (ρ, u, p).

- VFRoe

	First order	Second order
ρ	0.654	0.791
u	0.853	0.967
p	0.811	0.988

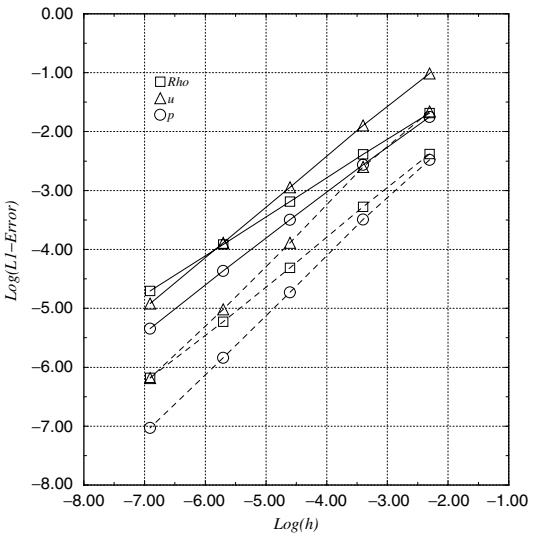

Figure 30. VFRoe ncv (τ, u, p).

- VFRoe ncv (ρ, u, p)

	First order	Second order
ρ	0.654	0.791
u	0.853	0.967
p	0.811	0.988

- VFRoe ncv (τ, u, p)

	First order	Second order
ρ	0.653	0.791
u	0.853	0.967
p	0.812	0.988

Perfect gas EOS—sonic rarefaction wave (Figures 31–36):

- Energy relaxation

	First order	Second order
ρ	0.890	0.810
u	0.933	0.973
p	0.927	0.995

- Rusanov

	1st order	2nd order
ρ	0.684	0.827
u	0.794	0.985
p	0.821	0.999

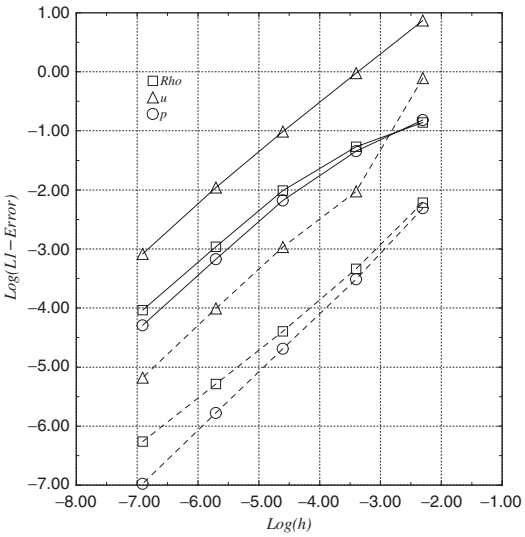

Figure 31. Energy relaxation.

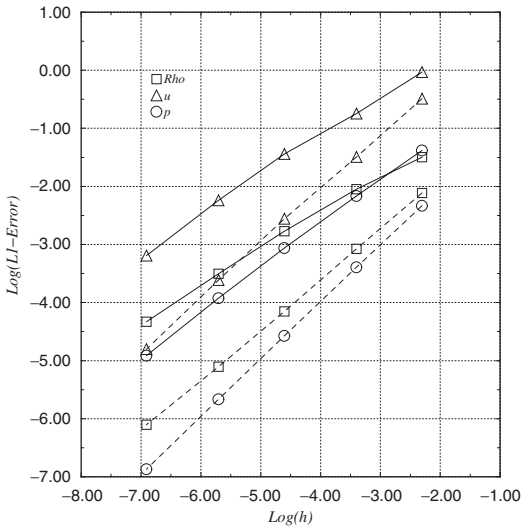

Figure 32. Rusanov.

- VFFC

	First order	Second order
ρ	0.667	0.819
u	0.808	0.977
p	0.798	0.996

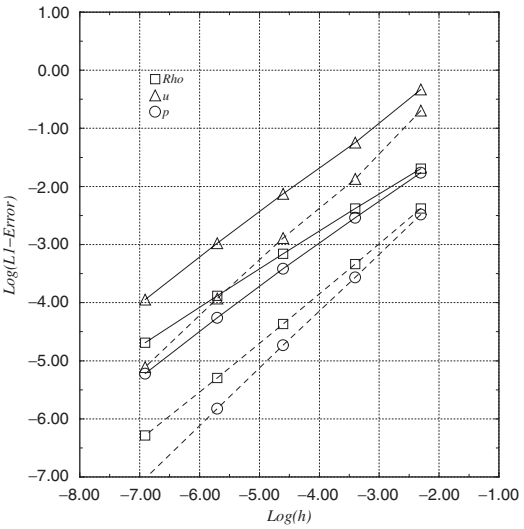

Figure 33. VFFC.

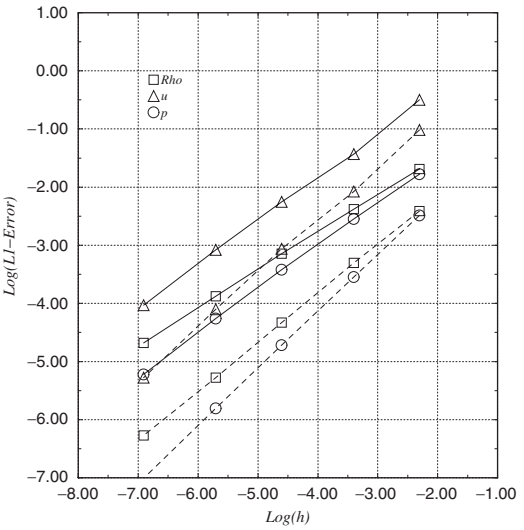

Figure 34. VFRoe.

- VFRoe

	First order	Second order
ρ	0.669	0.828
u	0.791	0.975
p	0.796	0.996

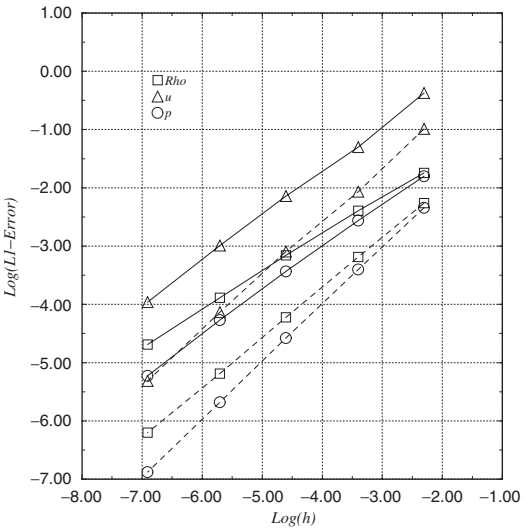

Figure 35. VFRoe ncv (ρ, u, p).

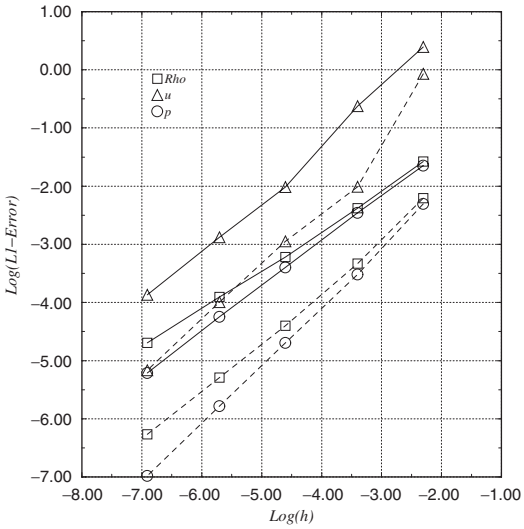

Figure 36. VFRoe ncv (τ, u, p).

- VFRoe ncv (ρ, u, p)

	First order	Second order
ρ	0.667	0.840
u	0.805	0.977
p	0.796	0.995

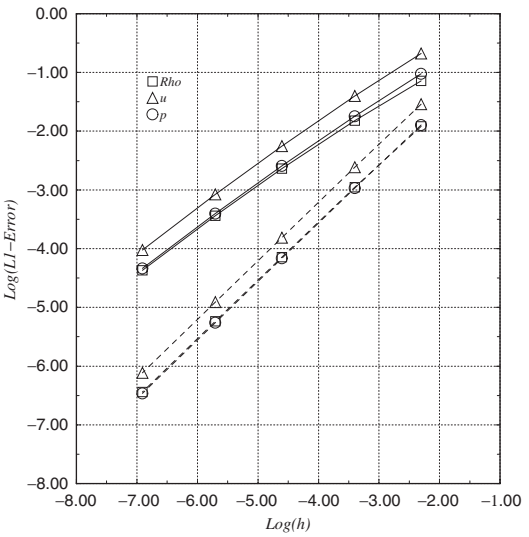

Figure 37. Energy relaxation.

- VFRoe ncv (τ, u, p)

	First order	Second order
ρ	0.653	0.809
u	0.822	0.973
p	0.802	0.995

Perfect gas EOS—symmetrical double rarefaction wave (Figures 37–42):

- Energy relaxation

	First order	Second order
ρ	0.771	0.998
u	0.785	0.999
p	0.775	0.999

- Rusanov

	First order	Second order
ρ	0.773	0.999
u	0.787	1.000
p	0.777	0.999

- VFFC

	First order	Second order
ρ	0.768	0.998
u	0.782	1.000
p	0.772	0.999

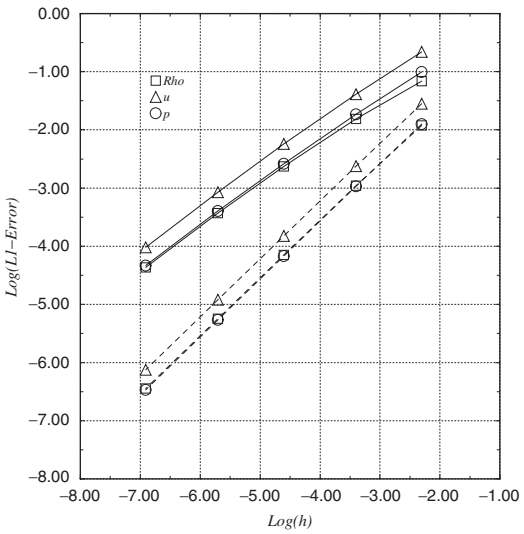

Figure 38. Rusanov.

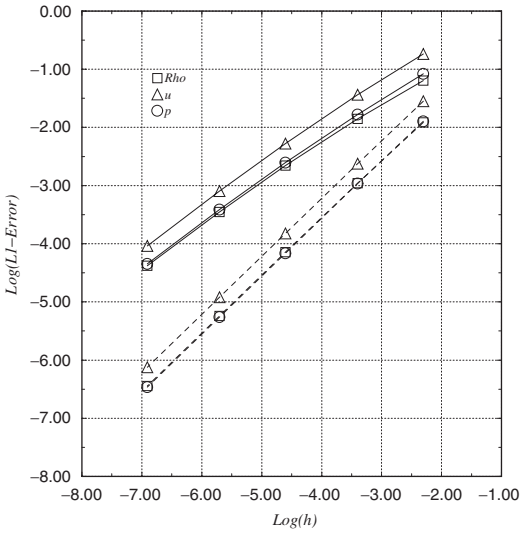

Figure 39. VFFC.

- VFRoe

	First order	Second order
ρ	0.771	0.998
u	0.785	0.999
p	0.775	0.999

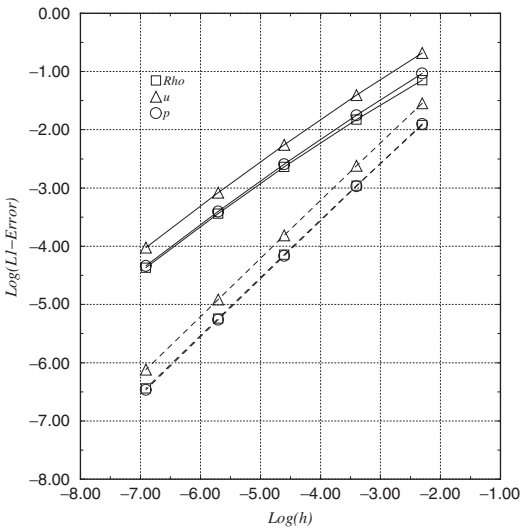

Figure 40. VFRoe.

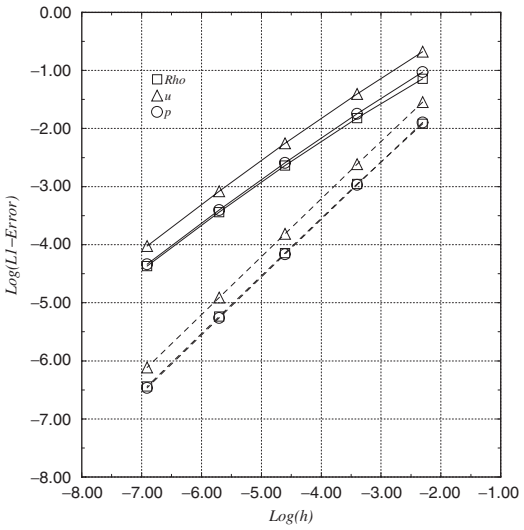

Figure 41. VFRoe ncv (ρ, u, p).

- VFRoe ncv (ρ, u, p)

	First order	Second order
ρ	0.771	0.998
u	0.785	0.999
p	0.775	0.999

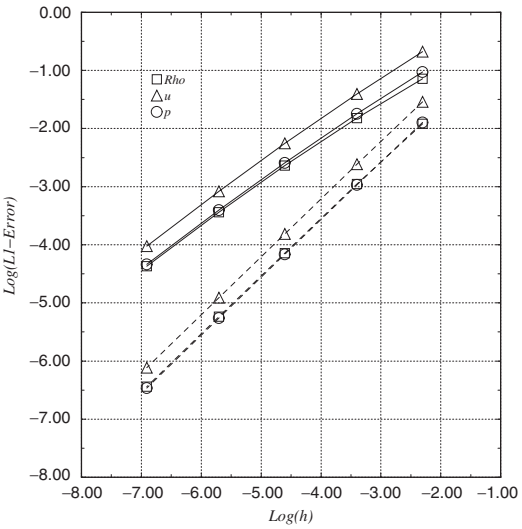

Figure 42. VFRoe ncv (τ, u, p).

- VFRoe ncv (τ, u, p)

	First order	Second order
ρ	0.771	0.998
u	0.785	0.999
p	0.775	0.999

Perfect gas EOS—symmetrical double shock wave (Figures 43–48):

- Energy relaxation

	First order	Second order
ρ	1.062	0.935
u	1.157	1.156
p	1.050	1.017

- Rusanov

	First order	Second order
ρ	1.060	1.028
u	1.056	1.115
p	0.996	1.001

- VFFC

	First order	Second order
ρ	1.060	0.905
u	1.157	1.154
p	1.049	1.019

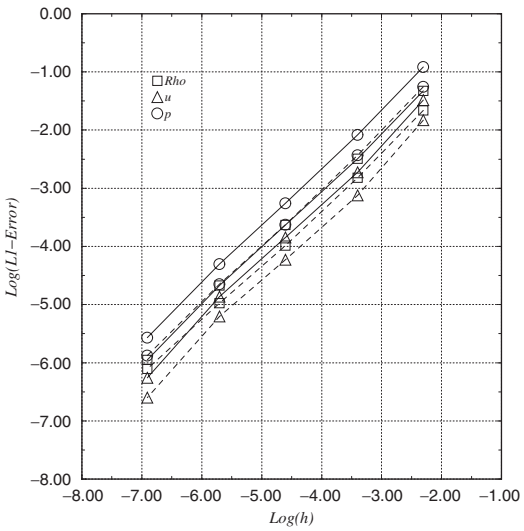

Figure 43. Energy relaxation.

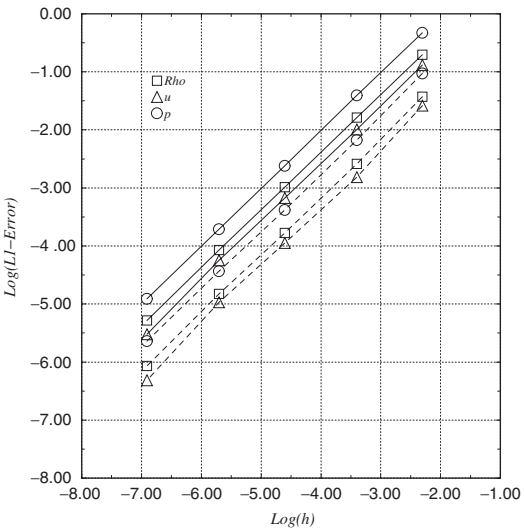

Figure 44. Rusanov.

- VFRoe

	First order	Second order
ρ	1.063	0.927
u	1.157	1.153
p	1.050	1.019

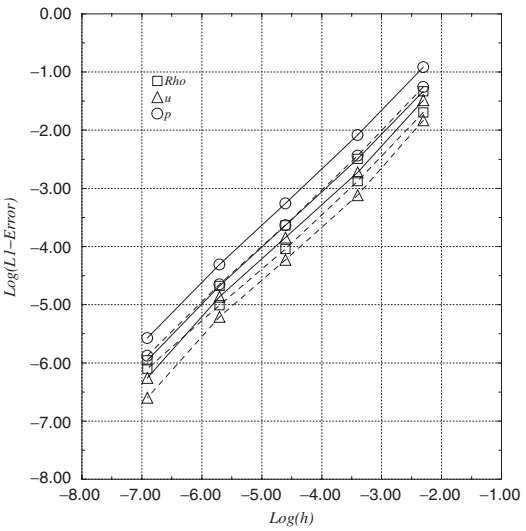

Figure 45. VFFC.

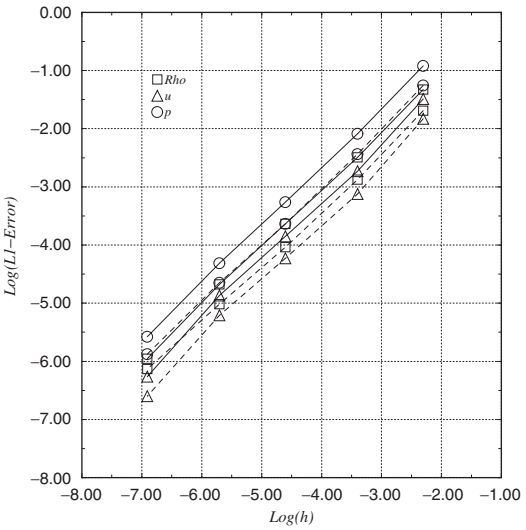

Figure 46. VFRoe.

- VFRoe ncv (ρ, u, p)

	First order	Second order
ρ	1.063	0.929
u	1.158	1.154
p	1.050	1.019

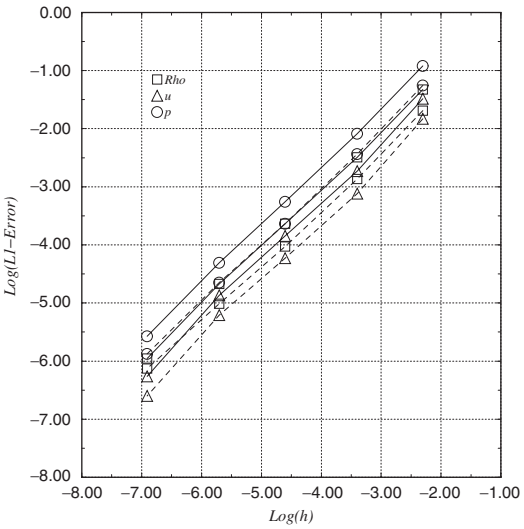

Figure 47. VFRoe ncv (ρ, u, p).

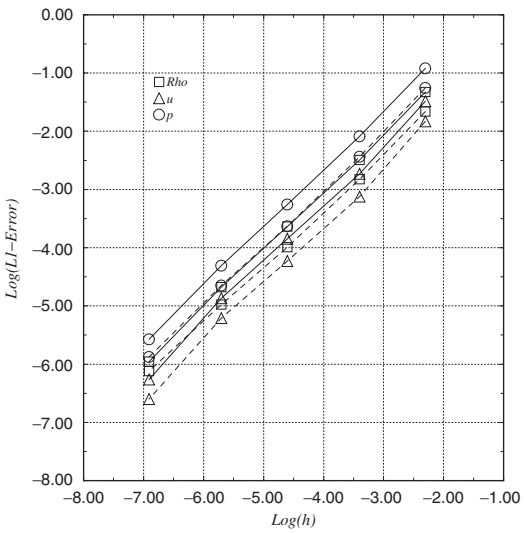

Figure 48. VFRoe ncv (τ, u, p).

- VFRoe ncv (τ, u, p)

	First order	Second order
ρ	1.062	0.947
u	1.157	1.153
p	1.050	1.019

Perfect gas EOS—unsteady contact discontinuity (Figure 49):

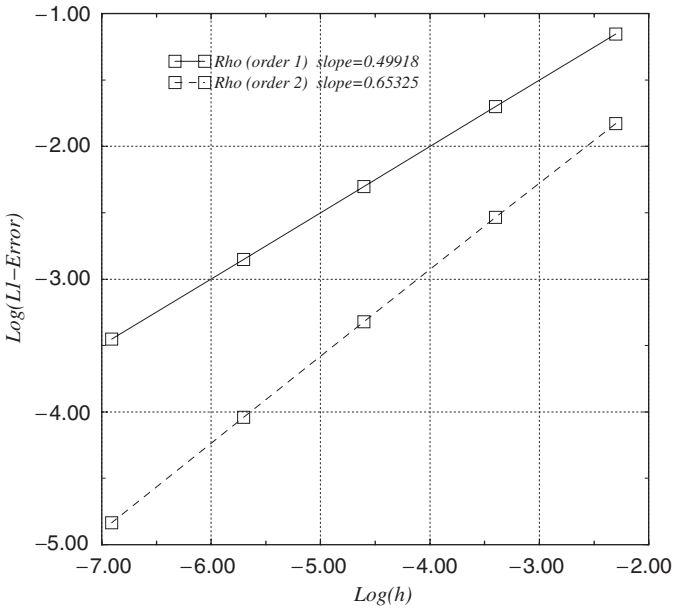

Figure 49. Case 2.1: density.

5. CONCLUSION

Several approximate Riemann solvers have been compared in this study. Some among them are based on an approximate Godunov scheme, applying various changes of variables in order to compute approximate values of state at the interface. These make use of conservative variable W, flux variable $F(W)$ or variable (ρ, u, p) or (τ, u, p). The latter enables to preserve unsteady contact discontinuties provided the EOS agrees with some conditions (perfect gas EOS, Tammann EOS belong to the latter class). The practical or theoretical behaviour of these schemes when computing steady shock wave, steady contact discontinuity, or vacuum has been investigated. All schemes perform rather well in all experiments, except in vacuum occurrence or propagation over vacuum. One drawback of the VFFC scheme can be emphasized: when computing a double supersonic rarefaction wave (with or without vacuum occurrence), this scheme blows up after a few time steps. Concerning VFRoe ncv (τ, u, p) and PVRS schemes, changing slightly the average state can increase their robustness and accuracy. The energy relaxation method applied with VFRoe ncv (τ, u, p) scheme has been computed too. The behaviour of this method is nearly the same as the original VFRoe ncv (τ, u, p) scheme. However, the energy relaxation method makes non-entropic shocks vanish. The Rusanov scheme provides good results too, though it is slightly less accurate than the other schemes investigated, due to important numerical diffusion. But the Rusanov scheme converges as fast as other schemes (in terms of mesh size exponent in the error norm). Moreover, it is the most robust scheme computed here, in particular in test cases with vacuum.

Moreover, a quantitative study has been presented. Solutions involving discontinuities have been investigated for first- and second-order schemes. Classical rates when restricting to

smooth solutions ($\mathscr{C}^\infty$) are around 1 and 2, respectively. When the solution contains rarefaction waves or shock waves (without contact discontinuities), the rate becomes less than or equal to (for the second-order schemes) 1. Restricting to a simple unsteady contact discontinuity, first-order schemes provide a rate around $\frac{1}{2}$ and second-order schemes provide a rate around $\frac{2}{3}$.

The framework of this paper has been restricted to the computation by finite volume schemes of a conservative and hyperbolic system, in one space dimension. Let us recall some extensions of the methods used here, in different applications.

Of course, all schemes presented herein can be extended to 2D or 3D problems (see Reference [28]). Rusanov (see Reference [6]), Godunov (see Reference [6]), VFFC (see Reference [9]) and VFRoe ncv (τ, u, p) (see Reference [12]) schemes have been applied to Euler equations with real gas EOS, shallow water equations (see Reference [2]) and compressible gas–solid two phase flows (see Reference [36]), with structured or unstructured meshes. Since these systems stay unchanged under frame rotation, a multi-dimensional framework may rely on a one-dimension method (see Reference [30]).

Some systems arising in CFD cannot be written under a conservative form, and thus, approximate jump relations must be proposed (see References [37, 38]). Some of the previous schemes have been extended to the non conservative formalism: Godunov (see References [38, 39]), Roe (see References [40–43]), VFRoe ncv (see References [6, 13, 14, 44]) and VFRoe (see Reference [4]).

Other non-conservative systems are conditionally hyperbolic, in particular when focusing on two-fluid two-phase flows (see Reference [45]). Three main directions have been proposed up to now in the literature. The first consists in splitting the Jacobian matrix into several matrices, which may be diagonalized in $\mathbb{R}$ (see Reference [46]). The second way consists in using the sign of the real part of eigenvalues to choose the flux direction (see References [9, 47]). A third approach is based on a development in power series of eigenvalues and eigenvectors in terms of a small parameter (see References [43, 48]).

APPENDIX A

A.1. Numerical preservation of velocity and pressure through the contact discontinuity in Euler equations

We discuss in this appendix about schemes and state laws, in order to preserve velocity and pressure on the contact discontinuity, in a one-dimension framework. We focus on initial conditions of a Riemann problem, with constant velocity and constant pressure. Schemes investigated here can be derived from the formalism of VFRoe ncv scheme, with variable

$$Y = {}^t(\varphi, u, p)$$

where $\varphi = \varphi(\rho, s)$ (s denotes the specific entropy) must be independent of pressure p (for instance, $\varphi = \rho, \tau, \ldots$).

Restricting to regular solutions, Euler equations can be written in relation to $Y = {}^t(\varphi, u, p)$ as follows:

$$Y_{,t} + A(Y)Y_{,x} = 0$$

where

$$A=\begin{pmatrix} u & \rho\varphi_{,\rho} & 0 \\ 0 & u & \rho^{-1} \\ 0 & \hat{\gamma}p & u \end{pmatrix}$$

At each interface, we linearize the matrix $A(Y)$ to obtain a linear Riemann problem, which may be easily solved. Initial conditions are defined by the average values in cells apart from the considered interface ($i+\frac{1}{2}$ for instance)

$$\begin{gathered} \frac{\partial Y}{\partial t}+A(\hat{Y})\frac{\partial Y}{\partial x}=0 \\ Y(x,0)=\begin{cases} Y_{\mathrm{L}}=Y(W_i^n) & \text{if } x<0 \\ Y_{\mathrm{R}}=Y(W_{i+1}^n) & \text{if } x>0 \end{cases} \end{gathered} \tag{A.1}$$

with $\hat{Y}$ such that $\hat{Y}(Y,Y)=Y$.
To compute the solution at the interface, we need to write the eigenstructure of the matrix $A(Y)$. As usual, the eigenvalues are (c stands for the sound speed)

$$\lambda_1=u-c, \quad \lambda_2=u, \quad \lambda_3=u+c$$

The associated right eigenvectors are

$$r_1(Y)=\begin{pmatrix} \rho\varphi_{,\rho} \\ -c \\ \rho c^2 \end{pmatrix}, \quad r_2(Y)=\begin{pmatrix} 1 \\ 0 \\ 0 \end{pmatrix}, \quad r_3(Y)=\begin{pmatrix} \rho\varphi_{,\rho} \\ c \\ \rho c^2 \end{pmatrix}$$

Left eigenvectors of $A(Y)$ are

$$l_1(Y)=\frac{1}{2c^2}\begin{pmatrix} 0 \\ -c \\ \rho^{-1} \end{pmatrix}, \quad l_2(Y)=\frac{1}{c^2}\begin{pmatrix} 1 \\ 0 \\ -\varphi_{,\rho} \end{pmatrix}, \quad l_3(Y)=\frac{1}{2c^2}\begin{pmatrix} 0 \\ c \\ \rho^{-1} \end{pmatrix}$$

In the following, we denote $\tilde{}$ variables computed on the basis of $\overline{Y}$. The solution of the linear problem (10), when $x/t\neq\lambda_k$, $k=1,2,3$, is

$$\begin{aligned} Y^*(x/t;Y_{\mathrm{L}},Y_{\mathrm{R}}) &= Y_{\mathrm{L}}+\sum_{x/t>\tilde{\lambda}_k}({}^t\tilde{l}_k(Y_{\mathrm{R}}-Y_{\mathrm{L}}))\tilde{r}_k \\ &= Y_{\mathrm{R}}-\sum_{x/t<\tilde{\lambda}_k}({}^t\tilde{l}_k(Y_{\mathrm{R}}-Y_{\mathrm{L}}))\tilde{r}_k \end{aligned}$$

Since the three eigenvalues of the linear system are distinct, two intermediate states Y_1 and Y_2 may occur

$$\begin{aligned} Y_1 &= Y_{\mathrm{L}}+\tilde{\alpha}_1\tilde{r}_1 \\ Y_2 &= Y_{\mathrm{R}}-\tilde{\alpha}_3\tilde{r}_3 \end{aligned}$$

with

$$\widetilde{\alpha_1} = -\frac{1}{2\tilde{c}}\,\Delta u + \frac{1}{2\tilde{\rho}\,\tilde{c}^2}\Delta p$$

$$\widetilde{\alpha_3} = \frac{1}{2\tilde{c}}\,\Delta u + \frac{1}{2\tilde{\rho}\tilde{c}^2}\,\Delta p$$

where $\Delta(.) = (.)_{\mathrm{R}} - (.)_{\mathrm{L}}$. Note that the two intermediate states Y_1 and Y_2 do not depend on the choice of φ.

Recall that initial conditions investigated herein are unsteady contact discontinuity. Thus,

$$\Delta u = \Delta p = 0 \Rightarrow \widetilde{\alpha_1} = \widetilde{\alpha_3} = 0$$

$$\Rightarrow Y_1 = Y_{\mathrm{L}} \text{ and } Y_2 = Y_{\mathrm{R}}$$

Note that these equalities are verified at each interface of the mesh. Hence, if we denote by $\rho_{i+1/2}$ the numerical density of problem (10) at the interface $i+\frac{1}{2}$, u_0 and p_0 the initial velocity and pressure, the finite volume scheme applied to the mass conservation equation gives

$$\begin{aligned}\rho_i^{n+1} &= \rho_i^n - \frac{\Delta t}{\Delta x}\left((\rho u)_{i+1/2} - (\rho u)_{i-1/2}\right)\\ &= \rho_i^n - \frac{\Delta t}{\Delta x}\,u_0(\rho_{i+1/2} - \rho_{i-1/2})\end{aligned}$$

Now, if we apply the finite volume scheme to the momentum conservation equation, it gives

$$\begin{aligned}(\rho u)_i^{n+1} &= (\rho u)_i^n - \frac{\Delta t}{\Delta x}\left((\rho u^2 + p)_{i+1/2} - (\rho u^2 + p)_{i-1/2}\right)\\ &= (\rho u)_i^n - \frac{\Delta t}{\Delta x}\left((\rho_{i+1/2}u_0^2 + p_0) - (\rho_{i-1/2}u_0^2 + p_0)\right)\\ &= (\rho u)_i^n - \frac{\Delta t}{\Delta x}u_0^2(\rho_{i+1/2} - \rho_{i-1/2})\\ &= u_0\left(\rho_i^n - \frac{\Delta t}{\Delta x}u_0(\rho_{i+1/2} - \rho_{i-1/2})\right)\\ &= u_0\rho_i^{n+1}\end{aligned}$$

Thus, we have $u_i^{n+1} = u_0,\ \forall i \in \mathbb{Z}$.

To study the discrete preservation of pressure, let us write the finite volume scheme applied to the energy conservation equation

$$\begin{aligned}E_i^{n+1} &= E_i^n - \frac{\Delta t}{\Delta x}\left((u(E + p))_{i+1/2} - (u(E + p))_{i-1/2}\right)\\ &= E_i^n - \frac{\Delta t}{\Delta x}\,u_0(E_{i+1/2} - E_{i-1/2})\end{aligned}$$

Energy is defined by $E=\rho\varepsilon+\frac{1}{2}\rho u^2$. Thus, we have

$$(\rho\varepsilon)_i^{n+1}=(\rho\varepsilon)_i^n-\frac{\Delta t}{\Delta x}u_0((\rho\varepsilon)_{i+1/2}-(\rho\varepsilon)_{i-1/2})$$

Let us assume that the equation of state can be written under the form

$$\rho\varepsilon=f(p)+b\rho+c \tag{A.2}$$

where b and c are real constants, and f an inversible function (for instance perfect gas EOS, Tammann EOS, etc.). If we introduce this equation of state in the previous equation, it gives

$$\begin{aligned}(f(p)+b\rho+c)_i^{n+1}&=(f(p)+b\rho+c)_i^n\\&\quad-\frac{\Delta t}{\Delta x}u_0((f(p)+b\rho+c)_{i+1/2}-(f(p)+b\rho+c)_{i-1/2})\\f(p_i^{n+1})+b\rho_i^{n+1}+c&=f(p_0)+b\rho_i^n+c\\&\quad-\frac{\Delta t}{\Delta x}u_0((f(p_0)-f(p_0))+b(\rho_{i+1/2}-\rho_{i-1/2})+(c-c))\\f(p_i^{n+1})&=f(p_0)\end{aligned}$$

Thus, $p_i^{n+1}=p_0$.

Hence, if a state law can be written under form (11), then a VFRoe ncv scheme with variable (φ,u,p) maintains velocity and pressure constant.

Moreover, if the contact discontinuity is steady (i.e. $u_0=0$), we can remark that the VFRoe ncv (φ,u,p) scheme preserves pressure and velocity exactly constant, whatever the state law considered.

REFERENCES

1. Seguin N. Comparaison numérique de schémas Volumes Finis pour les équations d'Euler en gaz parfaits et réels. *EDF-DRD Report HI*-81/00/010/A, 2000; 1–451 (in French).
2. Buffard T, Gallouët T, Hérard JM. A naive Godunov scheme to solve shallow-water equations. *C. R. Academy of Science Paris* 1998; **I-326**:885–890.
3. In A. Numerical evaluation of an energy relaxation method for inviscid real fluids. *SIAM Journal on Scientific Computing* 1999; **21**(1):340–365.
4. Masella JM. Quelques méthodes numériques pour les écoulements diphasiques bi-fluides en conduites pétrolières. *Ph.D. thesis*, Université Paris VI, France, May 1997.
5. Masella JM, Faille I, Gallouët T. On an approximate Godunov scheme. *International Journal of Computational Fluid Dynamics* 1999; **12**:133–149.
6. Xeuxet E. Comparaison de solveurs numériques pour le traitement de la turbulence bifluide. *Ph.D. thesis*, Université d'Evry, France, June 1999.
7. Gallouët T, Masella JM. A rough Godunov scheme. *C. R. Academy of Science Paris* 1996; **I-323**:77–84.
8. Ghidaglia JM, Kumbaro A, Le Coq G. Une approche volume fini à flux caractéristiques pour la résolution numérique des systèmes hyperboliques de lois de conservation, *C. R. Academy of Science Paris* 1996; **I-322**:981–988.
9. Boucker M. Modélisation numérique multidimensionnelle d'écoulements diphasiques liquide–gaz en régimes transitoire et permanent: méthodes et applications. *Ph.D. thesis*, École Normale Supérieure de Cachan, France, December 1998.
10. Kumbaro A. Schéma volume fini à flux caractéristiques—implémentation, tests et résultats numériques. *EDF-DER Report HT*-30/95/017/A, 1995 (in French).

11. Buffard T, Gallouët T, Hérard JM. Schéma VFRoe en variables caractéristiques. Principe de base et applications aux gaz réels. *EDF-DER Report HE*-41/96/041/A, 1996 (in French).
12. Buffard T, Gallouët T, Hérard JM. A sequel to a rough Godunov scheme. Application to real gas flows. *Computers and Fluids* 2000; **29**(7):813–847.
13. Buffard T, Gallouët T, Hérard JM. A naive Godunov scheme to compute a non-conservative hyperbolic system. *International Series of Numerical Mathematics* 1998; **129**:129–138.
14. Buffard T, Gallouët T, Hérard JM. An approximate Godunov scheme to compute turbulent real gas flow models. *AIAA paper* 99-3349, 1999.
15. Toro EF. A linearised Riemann solver for time-dependent Euler equations of gas dynamics. *Proceedings of the Royal Society of London A* 1991; **434**:683–693.
16. Toro EF. *Riemann Solvers and Numerical Methods for Fluid Dynamics*. Springer: Berlin, 1997.
17. Ivings MJ, Causon DM, Toro EF. On Riemann solvers for compressible flows. *International Journal of Numerical Methods in Fluids* 1998; **28**:395–418.
18. Rusanov VV. Calculation of interaction of non-steady shock waves with obstacles. *Journal of Computational Mathematics and Physics USSR* 1961; **1**:267–279.
19. Gest B, Hérard JM, Kloetzer L. Validation d'un algorithme implicite volumes finis pour gaz réels. *EDF-DER Report HE*-41/98/041/A 1998 (in French).
20. Coquel F, Perthame B. Relaxation of energy and approximate Riemann solvers for general pressure laws in fluid dynamics equations. *SIAM Journal on Numerical Analysis* 1998; **35**(6):2223–2249 (in memory of Ami Harten).
21. In A. Méthodes numériques pour les équations de la dynamique des gaz complexes et écoulements diphasiques. *Ph.D. thesis*, Université Paris VI, France, October 1999.
22. Rascle P, Morvant O. Interface utilisateur de Thetis—THErmodynamique en Tables d'InterpolationS. *EDF-DER Report HT*-13/95021B, 1995 (in French).
23. Kee R, Miller J, Jefferson T. Chemkin: a general purpose, problem independent transportable fortran chemical kinetics code package. *SAND Report* 80-8003, Sandia National Laboratories.
24. Saurel R, Abgrall R. A simple method for compressible multifluid flows. *SIAM Journal on Scientific Computing* 1999; **21**(3):1115–1145.
25. Gallouët T, Hérard JM, Seguin N. An hybrid scheme to compute contact discontinuities in Euler systems. *EDF-DRD Report HI*-81/01/011/A, 2001; submitted for publication.
26. Letellier A, Forestier A. Le problème de Riemann en fluide quelconque. *CEA-DMT Report* 93/451, 1993 (in French).
27. Godunov SK. A difference method for numerical calculation of discontinuous equations of hydrodynamics. *Matematicheskii Sbornik* 1959; **47**:271–300 (in Russian).
28. Buffard T. Analyse de quelques méthodes de volumes finis non structurés pour la résolution des équations d'Euler. *Ph.D. thesis*, Université Paris VI, France, 1993.
29. LeVeque RJ. Wave propagation algorithms for multidimensional hyperbolic systems. *Journal of Computational Physics* 1997; **131**:327–353.
30. Godlewski E, Raviart PA. *Numerical Approximation of Hyperbolic Systems of Conservation Laws*. Springer: Berlin, 1996.
31. Eymard R, Gallouët T, Herbin R. Finite volume methods. In *Handbook of Numerical Analysis*, vol. VII, Ciarlet PG, Lions JL (eds). North-Holland: Amsterdam, 2000; 729–1020.
32. Einfeldt B, Munz CD, Roe PL, Sjögreen B. On Godunov-type methods near low densities. *Journal of Computational Physics* 1991; **92**(2):273–295.
33. Harten A, Hyman JM. A self-adjusting grid for the computation of weak solutions of hyperbolic conservation laws. *Journal of Computational Physics* 1983; **50**:235–269.
34. Roe PL. Approximate Riemann solvers, parameter vectors and difference schemes. *Journal of Computational Physics* 1981; **43**:357–372.
35. Van Leer B. Toward the ultimate conservative difference scheme V. A second-order sequel to Godunov's method. *Journal of Computational Physics* 1979; **32**:101.
36. Combe L, Hérard JM. Principe du maximum pour un modèle diphasique gaz–solide à trois équations. *EDF-DER Report HE*-41/96/045/A, 1996 (in French).
37. Dal Maso G, Le Floch PG, Murat F. Definition and weak stability of non conservative products. *Journal de Mathematiques*, *Pures et Appliques* 1995; **74**:483–548.
38. Colombeau JF. *Multiplication of Distributions*. Springer: Berlin, 1992.
39. Forestier A, Hérard JM, Louis X. A Godunov type solver to compute turbulent compressible flows. *C. R. Academy of Science Paris*, 1997; **I-324**:919–926.
40. Brun G, Hérard JM, Jeandel D, Uhlmann M. An approximate Roe-type Riemann solver for a class of realizable second-order closures. *International Journal of Computational Fluid Dynamics* 2000; **13**(3):233–249.
41. Hérard JM. Solveur de Riemann approché pour un système hyperbolique non conservatif issu de la turbulence compressible. *EDF-DER Report HE*-41/95/009/A, 1995 (in French).

42. Hérard JM, Forestier A, Louis X. A non strictly hyperbolic system to describe compressible turbulence. *EDF-DER Report HE*-41/94/011/A, 1994.
43. Sainsaulieu L. Finite volume approximations of two phase-fluid flows based on approximate Roe-type Riemann solver. *Journal of Computational Physics* 1995; **121**:1–28.
44. Berthon C, Coquel C, Hérard JM, Uhlmann M. An approximate solution of the Riemann problem for a realizable second moment turbulent closure. *Shock Waves* 2002; **11**(4):245–269.
45. Sainsaulieu L. Contribution à la modélisation mathématique et numérique des écoulements diphasiques constitués d'un nuage de particules dans un écoulement de gaz. *Thèse d'habilitation*, Université Paris VI, France, 1995.
46. Combe L, Herard JM. Finite volume algorithm to compute dense compressible gas–solid flows. *AIAA Journal* 1999; **37**:337–345.
47. Mimouni S, Boucker M, Le Coq G, Ghidaglia JM. *et al.* An overview of the VFFC-methods and tools for the simulation of two-phase flows. *EDF-DER Report HT*-33/99/006/A, 1999.
48. Toumi I, Kumbaro A. An approximate linearized Riemann solver of a two-fluid model. *Journal of Computational Physics* 1996; **124**:286–300.

